Spring 2018

Kinetic Modeling of the Atmospheric Photooxidation of Reduced Sulfur and Nitrogen Compounds

Jesus Alejandro Berlanga
Western Kentucky University, jaberna888@gmail.com

KINETIC MODELING OF THE ATMOSPHERIC PHOTOOXIDATION OF REDUCED SULFUR AND NITROGEN COMPOUNDS

A Thesis
Presented to
The Faculty of the Department of Chemistry
Western Kentucky University
Bowling Green, Kentucky

In Partial Fulfillment
Of the Requirements for the Degree
Master of Science

By
Jesús A. Berlanga Narváez

May 2018

KINETIC MODELING OF THE ATMOSPHERIC PHOTOOXIDATION OF REDUCED SULFUR AND NITROGEN COMPOUNDS

Date Recommended 4/18/2018

Matthew Nee, Director of Thesis

Philip J. Silva

Jeremy Maddox

Dean, Graduate School 4/20/18 Date

This thesis is dedicated to my parents and brother who have constantly encouraged and supported me to take risks and overcome obstacles throughout my life. Also, my teachers and colleagues from WKU and previous institutions who have poured time and effort towards my growth. To the many all-nighters of studying and countless cups of coffee, and to my faithful savior Jesus Christ.

ACKNOWLEDGEMENTS

I would like to thank and recognize the work of my research advisor and educator Dr. Matthew Nee for his patience and guidance throughout my research and the opportunity to grow in my scientific experience. Also, to acknowledge our collaborators from USDA, Philip Silva and from UCR, Paul Van Rooy and Dr. David Cocker. Thanks to the WKU chemistry department and all its members, special recognition to Haley Smith, our department's go-to person for the students in need.

TABLE OF CONTENTS

LIST OF FIGURES

LIST OF TABLES

KINETIC MODELING OF THE ATMOSPHERIC PHOTOOXIDATION OF REDUCED SULFUR AND NITROGEN COMPOUNDS

Jesús A. Berlanga Narváez May 2018 80 Pages

Directed by: Matthew Nee, Philip Silva, and Jeremy Maddox

Department of Chemistry Western Kentucky University

Atmospheric aerosols encapsulate a wide variety of particles with different compositions, sizes and sources of origin. They also directly and indirectly affect climate by their interactions with sunlight, clouds, atmospheric chemical species, and even other suspended particles. To understand the atmospheric aerosol processes and the effects they have in global and regional climate is of utmost importance for the future establishment of environmental regulations and emission policies that affect aerosol precursor compounds in an effective and beneficial manner. In particular, aerosols are known to be formed from emissions from human activities, such as fossil fuel burning, agriculture, or concentrated animal feeding operations (CAFOs). Secondary organic aerosols (SOA) constitute a type of atmospheric aerosols that are formed from the atmospheric oxidation of organic compounds that are released from various sources into the atmosphere. Due to the complexity of the atmosphere and variability of its conditions, the direct study of SOA formation is a challenging task, but the implementation of atmospheric chamber facilities to study aerosol formation and growth under controlled conditions has provided a way to study the formation and growth of SOA. However, chamber experiments cannot study specific reactions or individual compounds from the aerosol formation mechanisms in isolation, they can only provide insight on what is produced and what it is produced from, and under what conditions. Thus, kinetic modeling of the mechanisms of gas-phase

atmospheric oxidation of the compounds of interest is used to develop reliable and accurate chemical models that will help have precise estimations and determine the mechanisms by which volatile organic compounds interact to produce aerosol particles. Dimethyl sulfide (DMS), dimethyl disulfide (DMDS) and trimethylamine (TMA) are three relevant atmospheric compounds, due to their emissions from many natural and anthropogenic sources and recent studies on emissions of these compounds from animal waste from CAFOs has triggered the interests on the study of SOA formation from these and other similar compounds. In this study, kinetic modeling of the atmospheric oxidation mechanisms of DMDS, DMS and TMA is used to simulate atmospheric chamber studies of aerosol formation to develop accurate models and help determine the mechanisms of aerosol formation.

1 Description of Atmospheric Aerosols

The atmosphere is composed mainly of a mixture of gases, including molecular nitrogen and oxygen, carbon dioxide, argon, and other trace gases. It also contains a wide variety of suspended particles that are ubiquitous in the air.[1] These particles are collectively called atmospheric aerosols. Although the existence and plausible effects of atmospheric aerosols were recognized in the 1970s, it was not until the 1990s when studies on these particles became of focus for the scientific community.[2] As more studies on atmospheric aerosols were performed, a greater awareness of the great impacts that green-house gas (GHG) emissions, especially of carbon dioxide, methane, nitrous oxide, chlorofluorocarbons, and ozone, have on the warming of the atmosphere and depletion of the ozone layer was attained. These examples led scientists at the time to look more closely at aerosols and provided context as to the impacts that human activities could produce on the Earth's atmosphere and made it clear that understanding atmospheric chemical processes and the effects of human activities on the global climate was of utmost importance for the future establishment of better emission policies.[3,4] Atmospheric aerosols can be solid, liquid or heterogenous mixtures, are suspended in the atmosphere, and vary greatly in their properties.[1] Aerosols are considered to be part of a two phase system with one phase being the particle (solid or liquid) and the other phase being the air (gas), in which they are suspended.[5] They originate from both natural and anthropogenic sources that can contribute directly to the total aerosol concentrations by direct emission of primary aerosols (PA) into the atmosphere or indirectly by incorporating chemical species that contribute to the formation of particles through atmospheric chemical reactions.[1,6,7] Secondary aerosols that form through atmospheric chemical reactions are classified as

secondary organic aerosols (SOA) and are known to form from sulfur and nitrogen containing precursor compounds. This is one of the aspects that motivated the study of gas-phase atmospheric oxidation of low volatility reduced organo-sulfur and aliphatic amine compounds.

1.1 Climate and Health Effects

In terms of their climate impacts, atmospheric aerosol particles play a role by scattering and absorbing solar radiation and by introducing cloud condensation nuclei (CCN), which affect the microphysical properties of clouds such as cloud albedo.[8] The primary direct effect of aerosols is a brightening of the planet when viewed from space, while the primary indirect effects are observed on clouds and include an increase in cloud brightness, change in precipitation and possibly an increase in lifetime.[9] Thus, the overall net impact of aerosols in climate is an enhancement of Earth's reflectance (shortwave albedo). This reduces the sunlight reaching the surface of the Earth, producing a net climatic cooling, as well as a redistribution of the radiant and latent heat energy deposited in the atmosphere. By 2007, studies had indicated that on average, the sum of direct and indirect top-of-atmosphere (TOA) forcing by anthropogenic aerosols is negative (cooling) of about -1.3 W m^{-2} (-2.2 to -0.5 W m^{-2}). This is significant compared to the positive forcing by anthropogenic GHGs (including ozone), about 2.9 ± 0.3 W m^{-2}.[10,11]

1.1.1 Direct Climate Effects

In comparison, the effects of aerosols, unlike the effects of GHG emissions, are likely a somewhat regional and temporal effect, given their local origination and distribution, which occurs mainly near and downwind of the sources of emission, and their short lifetimes.[8] These effects can alter atmospheric circulation and the water cycle,

including precipitation patterns, on a variety of length and time scales.[12] Any change in number, concentration or hygroscopic properties of such particles has the potential to modify the physical and radiative properties of clouds, altering cloud brightness and the likelihood and intensity with which a cloud will precipitate. Collectively, changes in cloud processes due to anthropogenic aerosols are referred to as indirect aerosol effects.[13] Figure 1.1 offers a schematic overview of direct and indirect effects of aerosols on climate.

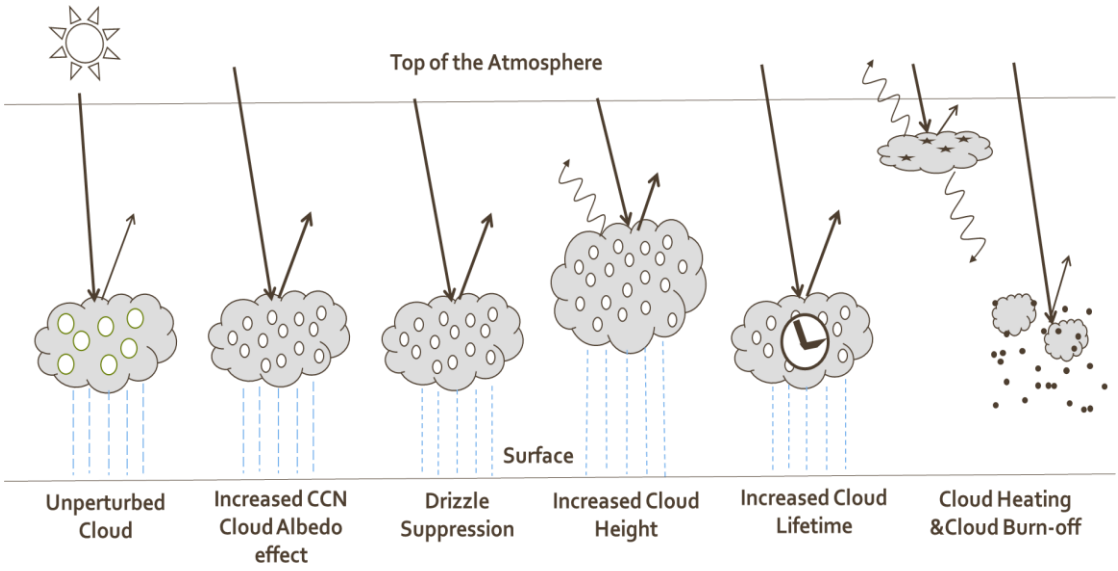

Figure 1.1. Direct and indirect effects of aerosol. Airborne particles can affect the heat balance of the atmosphere, directly, by scattering and absorbing sunlight, and indirectly, by altering cloud brightness and possibly lifetime. Small black dots represent aerosols, circles represent cloud droplets, straight lines represent short-wave radiation, and wavy lines represent long-wave radiation. Adapted from Ref. 13.

In Figure 1.1, aerosols scatter and absorb sunlight, described as direct effects on shortwave (solar) radiation. The second illustration represents a cloud in an unperturbed atmospheric state. The rest illustrate the different kinds of indirect effects of atmospheric aerosols, such as, increased CCN, rainfall suppression, increased cloud lifetime and height, and cloud burn-off. Most types of aerosols scatter more than 90% of the visible light

reaching them. This, leads to an increase in the amount of sunlight backscattering of the atmosphere, especially on regions of the atmosphere with highest concentrations of aerosols, which gives rise to an unbalance in the total radiative forcing of the Earth.

1.1.2 Indirect Climate Effects

Cloud microphysical and radiative properties such cloud lifetimes, droplet sizes and concentrations, volume and altitude are significantly affected by atmospheric aerosols. As observed in Figure 1.1, aerosols act as sites at which water vapor can accumulate during cloud droplet formation, serving as cloud condensation nuclei (CCN).[1,10] Increasing aerosol concentrations increases CCN for a given liquid water content, which increases back-scattering of sunlight, causing an enhancement of cloud albedo effect.[6,14] Studies have also related increased cloud lifetimes to indirect effects of aerosols. This consequence is linked to another one of those indirect effects of aerosols. Increased aerosols concentrations change the size of water droplets due to increased CCN concentrations, this is because cloud droplets need a threshold radius of approximately 14 μm for the formation of rain.[15] However, increased concentrations of CCN in clouds causes a decrease in droplet size and an increase in the number of droplets.[16] As a consequence, the droplets are prevented from reaching the threshold radius, which increases cloud lifetime and suppresses the rainfall.[6] Finally, absorption of solar radiation by particles is thought to contribute to a reduction in cloudiness, a phenomenon referred to as the semi-direct effect.[14] This occurs because aerosols warm up the space around them by absorbing sunlight, which changes the atmospheric stability, and reduces surface flux.[10] Size and composition of aerosol particles also determine their ability to serve as CCN, upon which cloud droplets form, which

provides an indirect relationship between aerosol sources and the aerosols ability to modifying cloud properties of certain aerosol types.

1.1.3 Health Effects

The most important effects of atmospheric aerosols in human health are caused by inhalation of air polluted with high concentrations of aerosols. Deposition and accumulation of such particles in the lungs and other parts of the respiratory system causes airway resistance or various diseases depending on their chemical composition.[6] The size of the particles plays a role in the impact that they can have on human health given that coarse particles, which have a diameter ranging from 2.5 μm to 10 μm are mainly removed in the upper respiratory track. However, particles with diameters less than 2.5 μm are deposited on the different parts of respiratory track all the way down to the bronchi walls. Particles smaller than 0.1 μm in diameter are collected in the bronchia through Brownian Motion. Particles with diameters between 0.1 -1 μm are deposited in the lungs as they are too large for Brownian Motion and too small to be trapped in the upper part of the trachea. Ultrafine particles (UFP) with sizes of <0.1 μm which are linked to increased risks of cardiovascular disease and pulmonary toxicity. [17–19] Thus, aerosols of smaller sizes likely represent a greater threat towards human health.

1.2 Aerosol Properties and Measurements

To study aerosols and their effect on global total radiative forcing and climate change in general, it is necessary to analyze certain properties of each type of aerosol individually as well as when heterogenous mixtures of them are present. Some of these properties relate to their interaction with solar and surface radiation, as well as their chemical composition and size. Some of the measurements that help scientists study aerosols include for example,

aerosol optical depth (AOD), single scattering albedo (SSA), surface albedo (SA), radiative forcing (RF) and the asymmetry parameter (g).

Formally, AOD is the integral of the product of particle number concentration and particle extinction cross-section (which accounts for individual particle scattering and absorption), along a path length through the atmosphere, and is a dimensionless quantity. SSA describes the fraction of light interacting with the particle that is scattered, compared to the total scattered and absorbed light. Values for SSA range from 0 to 1, for totally absorbing (dark) particles such as black carbon aerosols and for purely scattering ones respectively.[10] Surface albedo (A) is a measurement of reflectivity of the ground, ranges from 0 for purely absorbing to 1 for purely reflecting.[10] The asymmetry parameter (g), helps describe the kind of light scattering each type of aerosol promotes.[10] Radiative forcing (RF) is an important measurement that allows the quantification of the effects of aerosols on climate. RF is the net energy flux (downwelling minus upwelling) difference between an initial and a perturbed aerosol loading state, at a specified level in the atmosphere. This quantity depends on the specifications of the initial and perturbed aerosol states for which the radiative flux difference is calculated. Although there is still some uncertainty on current measurements, they have provided close estimates to what the effects of aerosols are on climate.

Other important aspect to consider is the size and composition distributions that atmospheric aerosols present. The extensive list of the different compositions and wide particle size range that aerosol particles exhibit makes studying aerosol impacts on climate and health a challenging task.[10] Aerosol particles show sizes that range from tenths of nanometers to tenths of micrometers, and are distributed spatially and temporally at

different concentrations. According to their size, aerosols are divided into two categories, *fine mode* and *coarse mode*, with diameters of less than 2.5 μm and greater than 2.5 μm respectively. Although this is the legal definition of fine and coarse mode, many scientists would argue the natural cutoff is ~1 μm. Two subcategories emerge from the fine mode aerosols, the Aitken nuclei mode ranging from 0.005 μm to 0.1 μm in diameter, and the accumulation mode, which has diameters between 0.1 μm to 2.5 μm. [6] In general, the mass to size distribution ratio of aerosols shows both fine and coarse mode aerosols resulting in a bimodal distribution, where particle number distributions peak at the fine mode, while particle mass distributions peak at the larger sizes (coarse mode). In remote areas with no anthropogenic sources near, coarse mode is dominant; while higher concentrations of fine mode aerosols are observed in areas with anthropogenic source dominance. The properties of size and composition are of special interest when studying the processes of aerosol formation and are properties used in this work to guide the development of the kinetic models. Particularly, the composition and concentration of sulfur and nitrogen compounds present in the aerosols are the focus of the kinetic modeling of dimethyl disulfide (DMDS), dimethyl sulfide (DMS) and trimethylamine (TMA).

1.3 Atmospheric Aerosols Sources

Because of the large number of sources, atmospheric aerosols exhibit a wide range of chemical compositions, which can include metals, salts, oxygenated organic compounds, and mixtures of these. Table 1.1 shows a list of some of the major sources of aerosols and their estimated yearly emission concentrations, lifetimes, and mass loading in the atmosphere.[10] It has also been observed that aerosols that have emissions sources near the earth's surface such as sea spray, biomass, particulate organic matter (POM), dust from

wind erosion, etc., usually show greater concentrations in the atmospheric boundary layer and decrease with altitude as they approach and go into the troposphere.[10]

Table 1.1. Estimated yearly emission, lifetime and mass loadings of major Aerosol types from Aerosol Models. BC= black carbon; POM = particulate organic matter. Adapted from Ref. 10.

Aerosol Type	**Total source (Tg^{1}/yr)**	**Lifetime (day)**	**Mass loading (Tg^{1})**
	Median (range)	Median (range)	Median (range)
Sulfate[2]	190 (100-230)	4.1 (2.6-5.4)	2.0 (0.9-2.7)
BC	11 (8-20)	6.5 (5.3-15)	0.2 (0.05-0.5)
POM[2]	100 (50-140)	6.2 (4.3-11)	1.8 (0.5-2.6)
Dust	1600 (700-4000)	4.0 (1.3-7)	4.0 (1.3-7)
Sea Salt	6000 (2000-120000)	0.4 (0.03-1.1)	0.4 (0.03-1.1)

In a few cases, when the emissions occur above the boundary layer, aerosols can be lofted to higher elevations, which leads to increased atmospheric lifetimes, allowing the opportunity for a greater impact in climate. These occurrences include smoke from wildfires and volcanic effluent. Two notable examples are the eruption of Mt. St. Helen in 1980 and its effect on the region's climate afterwards,[20] and the sulfuric acid formed by the 1991 Pinatubo eruption, which exerted a measurable effect on the atmospheric heat budget for several years thereafter.[10]

1.3.1 Natural Sources

There is a wide variety of natural sources for aerosols. Natural sources include any naturally occurring source of particulate matter and of VOC emissions, and, as seen in Table 1.1, dust and sea salt are the major contributors of total aerosols concentrations. However, other sources, such as sulfates and black carbon are estimated to have more

impactful effects of the total change on Earth's reflectivity. The oxidation of atmospheric VOCs from biogenic emissions also referred to as biogenic volatile organic compounds (BVOCs), which include isoprene (2-methyl-1,3-butadiene) and monoterpenes, significantly contribute to the global SOA budget.[21] Those BVOCs have high reactivity with atmospheric oxidants, such as hydroxyl radicals (OH), ozone (O_3), and nitrate radicals (NO_3), and their large global emission rates makes their contribution towards SOA formation essential.[22] Among the different types of natural sources of atmospheric aerosols are biogenic aerosols, which consist of plant debris, humic matter and microbial particles, such as bacteria, fungi, viruses, spores, pollen, etc. This category of natural sources includes naturally occurring emissions from forested areas, which release aromatic compounds or BVOCs, contributing in this way to the concentration of atmospheric aerosols.[5] Dust from soil is another important natural source. It is emitted mainly from arid regions such as deserts, dry lake beds, and semi-arid desert fringes, as well as regions where vegetation has been reduced or soil surfaces have been disrupted by human activities. Dust is a major contributor to aerosol leading mass and optical thickness, particularly in tropical and sub-tropical regions.[5] However, as seen from Table 1.2, aerosols also form from various physical processes occurring near and at the marine surface, especially from the bursting of air bubbles during whitecap formation, which frees fine particulates of sea salt or organic matter.[23]

The largest contributions to natural aerosols are estimated to come from marine emissions; as shown in Table 1.2, sea salt and mineral dust are the most abundant of the natural emissions.[23] Volcanic emissions, although they are not constant, can also play a significant role in climate change.[24] Emissions from volcanic activity include volcanic dust

(ashes) and gaseous sulfur compounds such as dimethyl sulfide (DMS) and sulfur dioxide are released from volcanic emissions.[5]

Table 1.2. Emissions of atmospheric aerosols and their aerosol precursors from natural sources. Reproduced from Ref. 10.

Natural sources of aerosols	Global Natural Emissions (Tg yr^{-1})
Marine primary organic aerosols (POA)	2-20
Dimethyl sulfide (DMS)	10-40
Spores	28
Monoterpenes	30-120
SOA production BVOCs	20-380
Isoprene	410-600
Terrestrial bioaerosols	50-1000
Mineral dust	1000-4000
Sea spray	1400-6800

1.3.2 Anthropogenic Sources

In 2006 it was estimated that about 10% of global atmospheric aerosol mass was generated by human activity.[10] More recent studies have shown that the effects of atmospheric aerosols are only temporary and somewhat regional, meaning they are contained in the immediate vicinity and downwind of the source's origin.[8,10] Anthropogenic aerosols originate from urban and industrial emissions, domestic fire and other combustion products, smoke from agricultural burning, and soil dust created by overgrazing, deforestation, draining of inland water bodies, some farming practices, animal feeding operations, and generally, land management activities that destabilize the surface,

facilitating wind erosion of soils.[10,25] Some of the major species of anthropogenic aerosols include black carbon (BC), sulfate aerosols and organic carbon (OC).

1.3.2.1 Black Carbon

Black carbon is a type of primary aerosol that is directly emitted from incomplete combustion processes such as fossil fuel and biomass burnings, which are anthropogenic processes. These processes are also related to the emission of reduced sulfur organic compounds and SO_2. Global emissions of BC during the period from 1950 to 1090s estimated about 8.0 TgC yr^{-1} with contributions of 4.6 Tg yr^{-1} and 3.3 TgC yr^{-1} from fossil fuels and biomass respectively.[10,26] However, further emission controls from after this period have proved to help reduce the emissions of BC aerosols. This kind of aerosol strongly absorbs direct sunlight radiation, and studies have shown that BC has significantly absorbs surface radiation, while absorbing much less direct radiation; showing a local surface forcing of -23 W m^{-2}, which is significantly stronger than the -7 W m^{-2} for the local RF at the top of the atmosphere (TOA). Another characteristic of BC emissions is the complex chain structures in which it is emitted, those structures are known to break down after time with exposure to radiation and other atmospheric processes.[5] The interactions between black carbon, which are incompletely combusted organic compounds, and sulfate aerosols is also a possible source of SOA, as they interact in the atmosphere and undergo new particle formation processes.

1.3.2.2 Sulfate and Reduced Sulfur

Atmospheric sulfate aerosols are a secondary type of aerosol and are formed by aqueous phase reactions of SO_4^{2-} with cloud droplets. They may be considered as consisting of sulfuric acid particles that are partly or totally neutralized by ammonia and that are

present as liquid droplets. Like BC aerosols, fossil fuel burning is the main source of its kind, and it accounts for over 72% of the global emissions.[11] The process of formation begins by the oxidation of gaseous SO_2 into sulfate ions *via* gas-phase reactions with atmospheric species such as OH, NO_x, and O_3. Other emission sources of SO_2 include biofuel burning, biomass burning, marine phytoplankton emissions, and volcanic emissions. Volatile organosulfur compounds such as DMS and DMDS also contribute to the formation of these aerosols through atmospheric oxidation into SO_2, through similar atmospheric processes as the oxidation of SO_2 into sulfate ions. Studies have estimated a reduction of global anthropogenic emissions of sulfur from 73 to about 54 TgS yr^{-1} from 1980s to 2000s.[27] However, sulfate aerosols are still a concern to public health in some areas of the world with high industrial activities. For example, some regions of China where SO_4^{2-} is one of the dominant chemical components of particles with diameters of ≥ 2.5 μm. Cities like Shanghai, Beijing and Hong Kong typically exceed the World Health Organization (WHO) annual air quality guideline of 10 μg m^{-3} for $PM_{2.5}$.[28–31] The emissions from concentrated animal feeding operations (CAFOs) have also become of great concern as a source of reduced sulfur compounds (RSCs) and therefore of SOA sources in the last decades due to the increase in livestock production and changes in the production methods.[32] Early estimations from the 1980s estimated an annual emission of 16100 MT of sulfur compounds including dimethyl sulfide (DMS), carbonyl sulfide (COS), hydrogen sulfide (H_2S), carbon disulfide (CS_2), and dimethyl disulfide (DMDS).[33] Recent studies on the emission of RSCs from swine farms have shown that emissions from these operations are in great part H_2S, CH_3SH, DMDS and DMS. With concentrations

ranging from 30–200 ppb for H_2S, 2.5–20 ppb for CH_3SH, 1.5–12 ppb for DMS and 0.5–7 ppb for DMDS.[34]

Because of the importance of sulfur containing compounds in the generation of SOA, it is critical to continue the study of sulfate aerosol formation processes as well as the formation of SOA from heterogenous gas mixtures, specifically from reduced sulfur compounds which are emitted from CAFOs, such as DMS and DMDS.

1.3.2.3 Organic Carbon

Organic aerosols consist of complex mixtures of organic compounds containing C–C bonds produced from fossil fuel and biofuel burning as well natural biogenic emissions. They can be directly emitted as primary organic aerosol (POA) or form secondary organic aerosol (SOA) particles from condensation of organic gases considered semi-volatile or having low volatility. Hundreds of different atmospheric organic compounds have been detected in the atmosphere, which makes definitive modelling of the direct and indirect effects extremely challenging. Recent studies suggested that emissions of OC from anthropogenic sources range from 5 to 17 TgC yr^{-1}, with fossil fuel contributing only 2.4 TgC yr^{-1}. In contrasts to BC, the total radiative forcing of organic carbon aerosols from fossil fuel burning is estimated to be about –0.10 W m^{-2}. A difference in absorptivity is also observed between particles originated from fossil fuel burning and from biomass burning, with the OC from open biomass burning absorb more readily.[11] The burning of fossil and bio-fuels contribute greatly to the total aerosols loading. These activities contribute towards OC, BC, and sulfate aerosol formation.

These contributions are particularly impactful towards the formation of secondary organic aerosols and some warming of the atmosphere in regions near these sources due to

the absorptivity properties of BC and Organic aerosols.[11] As shown in Table 1.3, fossil fuels are responsible for most of the sulfur aerosols, producing an estimated 98.9 Tg yr^{-1}, which accounts for over half of the total estimated sulfur aerosol loading (Table 1.1), while biomass burning produces significantly larger emissions of POM. Another important anthropogenic source are the emissions from agricultural and animal waste, which contain high concentrations of OC, as well as reduced sulfur and nitrogen containing compounds.[35] DMDS, DMS and TMA are specifically some of these compounds generated from these emissions, and studying the mechanisms of atmospheric oxidation and aerosol particles.

Table 1.3 Anthropogenic emissions of aerosols and precursors for 2000. BC= black carbon; POM = particulate organic matter; S= sulfate. Adapted from Ref. 6.

Source	**Species[a]**	**Emission[b] (Tg/yr)** **2000**
Biomass burning	BC POM S	3.1 34.7 4.1
Biofuel	BC POM S	1.6 9.1 9.6
Fossil fuel	BC POM S	3.0 3.2 98.9

1.3.3 Mechanisms of Aerosol Removal

Aerosols are removed from the atmosphere primarily through cloud processing and wet deposition in precipitation, a mechanism that establishes average tropospheric aerosol atmospheric lifetimes at a week or less as can be observed in Table 1.1. Aerosols are also removed by dry deposition processes: gravitational settling tends to eliminate larger particles, impaction typically favors intermediate-sized particles. A third mechanism for

aerosol deposition consist of aerosol coagulation, where smaller particles can aggregate with larger ones, leading to their eventual deposition by wet or dry processes.[8,10]

The wet removal rate coefficients generally increase with the solubility and uptake by rain droplets and transfer to cloud droplets depend also on aerosol size. The solubility of aerosol types increases as follow:

Dust < BC < POM < Sulfate < Sea Salt

Dry deposition pathways increase with the particle sizes for particles larger than a few tens of microns, but sedimentation becomes increasingly faster than other dry deposition processes for larger particles of diameters larger than 5 microns.[8]

1.4 Climate Models and Aerosol Estimation Methods

The possible effects of aerosols have been recognized and studied for over four decades, however, due to their complex interactions with changes in their environment, including different compositions, years of preliminary studies and efforts to understand the aerosols properties and effects had to be made.[4,36] Today, POA and SOA still cannot be directly measured by chemical analysis methods, but they can be estimated by indirect approaches and by the advances in the techniques of measurements. The improvements in POA/SOA understanding of their origin, properties and concentrations have allowed global climate models to successfully incorporate effects of atmospheric aerosols into their parameters. Common methods include the EC tracer method, chemical mass balance (CMB) model, and chemical transportation model (CTM).[10,37,38] The EC tracer method is the simplest one which is often used. In this method, the ratio of OC/EC for POA is assumed to be a relatively stable representative value. The ambient ratio of OC/EC

exceeding the representative value is attributed to SOA. However, the ratio of OC/EC varies among the emission sources. Consequently, it was temporally and spatially unique and influenced by the meteorological and temporal fluctuation, which would lead to the large uncertainty for SOA estimation.[37] The CMB model requires the primary source profile as input for apportioning, so the unresolved OM is considered to be SOA. In this approach, the accuracy and integrity of sources profile influences the SOA estimation.[37] A more complete approach to the simulation of SOA is done with CTM, this model requires the detailed emission inventories of VOCs and formation mechanism of SOA. This method is limited by the current unclear knowledge of SOA formation and the uncertainty of the emission inventories.[37] In this area is where the studying of SOA formation processes using kinetic modeling and atmospheric chamber experiments can greatly contribute towards developing more accurate climate models that will reproduce and predict the impacts of atmospheric SOA on the earth's climate and atmosphere.

1.5 Secondary Organic Aerosols

Secondary organic aerosols are a special type of atmospheric aerosol that is formed from the atmospheric oxidation of volatile organic compounds.[39] The oxidation of these compounds leads to secondary organic aerosol (SOA) formation through low-volatility products that partition into the aerosol phase. Known SOA precursors include volatile organic sulfur and nitrogen containing compounds as well as volatile organic compounds such as terpenes, monoterpenes, etc.[40] A schematic representation for the formation of SOA is presented on Figure 1.2, where the volatile organic compounds are oxidized photolyzed by sunlight radiation ($h\nu$) and oxidized by atmospheric oxidizers (OH, NO_x, O_3) which lead to formation of other high volatility and semi-volatile products. Those semi-volatile

products, then either interact between them and undergo nucleation, or are partitioned further and form nuclei when they come in contact with cloud droplets. For example, the generation of organosulfates in laboratory generated SOA produced from the oxidation of BVOC's in the presence of an acidic sulfate seed aerosol, promote the formation of larger aerosol particles, which are more likely to undergo deposition processes.[29]

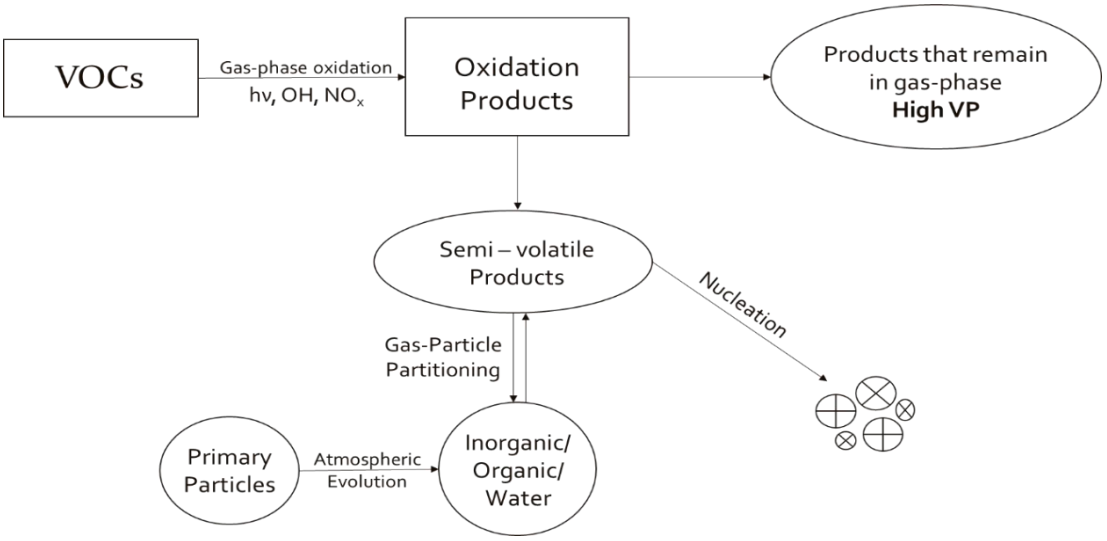

Figure 1.2 Route of formation of secondary organic aerosols. Products of sufficiently low volatility or "semi-volatile", are oxidized in the atmosphere, then some of the oxidized products stay in the gas-phase (high volatility products) while others may condense on pre-existing particles or nucleate homogeneously to form new particles. Reproduced from Ref. 17.

1.5.1 Organosulfate Precursors

Organosulfur compounds that are emitted from different anthropogenic and natural sources such as DMS and DMDS are oxidized in the atmosphere and produce SO_2 along with other compounds such as dimethyl sulfoxide (DMSO) and methanesulfonic acid (MSA). DMDS and DMS are the focus of this work, as they are known lead to the formation of SO_2, which is further oxidized into sulfate ions through interactions with

cloud droplets in the aqueous phase, which produces a phase change from gas to aqueous. The sulfate ions then interact with these droplets and other charged or polar compounds that might already be at or near the surface of the droplet. These interactions are still not well understood and are cause of some uncertainty and inaccuracy that current aerosol models face today. Chart 1.1 shows chemical structures of relevant organosulfur compounds.

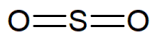
Sulfur dioxide

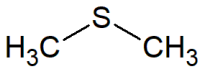
Dimethyl sulfide

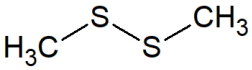
Dimethyl disulfide

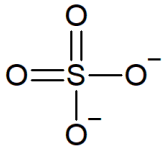
Sulfate ion

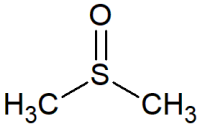
Dimethyl sulfoxide

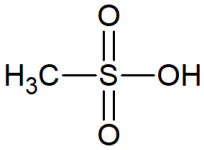
Methanesulfonic acid

Chart 1.1. Chemical structures of relevant atmospheric organosulfur compounds.

1.5.2 Nitrogen Precursors

Until recently, sulfate was the only species known to contribute to particle growth. However, parallel measurements of nanoparticle growth rates and H_2SO_4 show that sulfate typically accounts for only 5% to 50% of the observed growth.[41] This suggests that other species are contributing to post-nucleation growth**.** An extensive laboratory study of aliphatic amines focused on the roles of both salt formation and oxidation chemistry in gas-particle partitioning confirmed that gas-phase oxidation of the amine alkyl groups can lead to low-volatility oxidation products that can physically partition into particles.[42] Recent

field measurements of sites downwind of bovine sources in Riverside, and in the Central Valley region of California have shown that aminium salt formation occurs in aged organic carbon particles. [43,44] A variety of amines are emitted into the atmosphere from natural as well as anthropogenic sources. These compounds are emitted from oceans, biomass burning, vegetation, geologic activities and many current large scale industrial processes, which likely have fugitive emissions. Some examples of the use of amines in industry include their large use in the pharmaceutical industry. They are also widely used for crop protection, medication, and water purification. Amines are also used in a diverse array of end-use applications such as personal care products, cleaning products, gas treatment, petroleum and food processing.[10,37] Amine compounds are also used extensively in the foundry industry whereby their first use dates to the 1960s with the introduction of the phenolic urethane cold box process (PUCB). Trimethylamine (TMA), dimethylethylamine (DMEA) and dimethylisopropylamine (DMIPA) are commonly used in these processes.[45] The large use of amines results in direct and indirect emissions to the atmosphere and water supplies, making them have an important impact on aerosol formation. According to recent studies, approximately 150 amines have been identified in the atmosphere, and aliphatic amines of low molecular weight, containing within 1 to 6 carbons, have been found to me the most abundantly present. The emissions of aliphatic amines and NH_3 produced from animal waste, mainly from livestock and CAFOs also constitute a relevant source of nitrogen precursors that contribute to the formation of atmospheric aerosols.[35] Studies of emissions from animal husbandry showed that a global estimate of 0.15 ± 0.06 Tg y^{-1} of N-methylamine compounds such as methylamine (MA), dimethylamine (DMA) and TMA, were emitted strictly from agricultural sources, with TMA accounting for ~75% of these

emissions.[26] These emissions of amines and NH_3 undergo heterogenous uptake which allows for NPF processes or are atmospherically oxidized through photooxidative pathways or by reactions with OH radicals, and other oxidizers such as O_3 or NO_x species.[45,47–49] TMA and its gas-phase oxidation is one of the emphasis of this thesis.

1.5.3 Sulfur and Nitrogen Mixtures

Interactions between sulfur containing compounds and aliphatic ammines produced from animal waste and AFOs is a not a well understood area of aerosol formation. From previous studies of these interactions, it is suggested that heterogenous uptake of aliphatic amines by other particles is a likely pathway that enhances the formation of SOA.[45,48–50] However, because of the presence of many other species in the atmosphere and in these cloud droplets, the direct study of secondary organic aerosols from heterogenous mixtures of atmospheric emissions is particularly challenging. As a result, the use of atmospheric chamber experiments and kinetic modeling of gas-phase atmospheric oxidation of sulfur and nitrogen compounds such as DMDS, DMS and TMA has become an avenue by which the study of these heterogenous SOA formation processes can be done in a molecular level. An example of this is the use of chamber experiments to observe how the formation of aerosol particles is enhanced when MSA, an amine, and water are present in a heterogenous mixture.[47,51] These chamber studies found that the concentrations of particles formed from the mixing of MSA+TMA+H_2O increased by two orders of magnitude, from around 1.0×10^4 for mixtures of only MSA+H_2O and MSA+TMA to around 1.25×10^6 for mixtures of MSA+TMA+H_2O. Studies with NH_3, trimethylamine (TMA), dimethylamine (DMA), diethylamine (DEA), methylamine (MA), as well as other relevant amines have been done in this area as well.[27,45,48–51]

1.6 Study of Secondary Organic Aerosols

The complexity of the atmosphere, including wind directionality, humidity, and temperature changes, and the non-uniform distribution of aerosol concentrations make the direct studying of SOA formation processes especially challenging.[10,38,52] Thus, field observations are used to learn what is relevant on particle growth and laboratory experiments to better understand those processes. For this reason, using experimental instruments to closely resemble atmospheric conditions while allowing control and uniformity is essential to accurately study those processes. One experimental instrument that allows to study the formation of aerosol particles offering control over temperature, humidity, and other fluctuating atmospheric conditions is an atmospheric chamber facility.

1.6.1 Atmospheric Chamber Studies

Atmospheric chamber experiments provide the opportunity to study aerosol formation and growth under controlled experimental conditions. These experiments combine the challenges of both gas-phase chemistry and aerosol formation.[6] One of the principal goals of chamber-based atmospheric aerosol research is to understand the fundamental mechanisms by which gas-phase atmospheric chemistry leads to aerosol formation. Measurements required in such experiments include gas-phase species concentrations and aerosol size distribution and composition. Other aerosol microphysical properties measurements, such as hygroscopic water uptake, are also useful.[24] Atmospheric chamber experiments have shown to be useful in the study of SOA formation from relevant organic compounds. However, recent studies involving the formation of SOA from several low-volatility amine compounds has shown that these compounds adsorb onto the walls of the chamber facility. This leads to interferences with the experiment's results.[53,54]

However, these experiments allow studies to be performed at controlled temperatures, controlled relative humidities, and with a uniform and unvarying photolysis source. This photolysis rate consists of black-light lamps that provide light in wavelengths similar to sunlight.[52,55] As shown in Figure 1.3, the chamber allows the collection of real-time samples from inside the Teflon® walls through an outlet located on one of the walls to be analyzed by the instruments. The chamber also allows the injection of gases of interest, such as DMDS, DMS, and TMA, into the chamber through an inlet. Because the chamber is in a room with temperature controls, the temperature around and inside the chamber is kept relatively unchanged throughout the process of the experiments. This eliminates the varying temperatures, as well as the fluctuations of winds and humidity, which are challenges conveyed by direct studying of aerosols in the atmosphere. However, atmospheric chamber experiments only help eliminate some of the challenges that come with studying the mechanisms for aerosol formation. Even with chamber experiments it is still not possible to study specific reactions that might possibly be part of this mechanism in isolation. They can only provide with insight on what is produced and what it is produced from, and under what conditions. In other words, atmospheric chamber experiments can only tell what amounts and contents of aerosol particles are produced from a given initial gas-phase compound(s). They cannot tell much about the how these particles are formed, or the steps it takes to create them. An accurate predictive capability based on molecular-level understanding is critical for projecting the impacts of particles and developing optimal control strategies for future environmental regulations.[47] For this reason, it is key to understand how gas phase precursors leads to the formation and growth of new particles. Current models for one of the most studied systems, the conversion of gas-phase SO_2 to

sulfuric acid and sulfate particles, still typically underestimates particle formation by an order of magnitude or more.

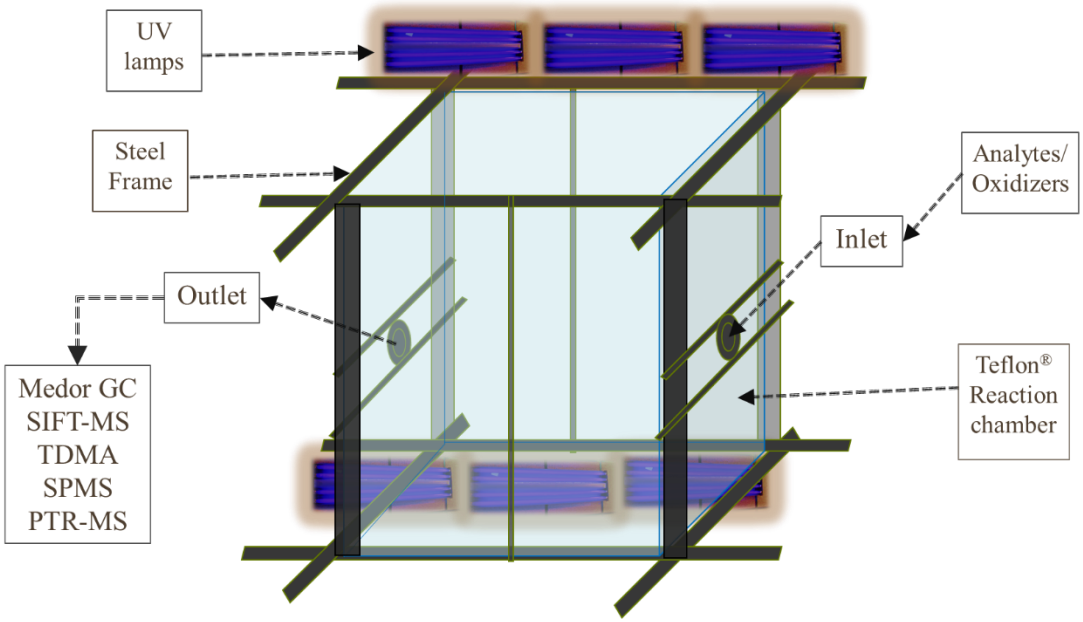

Figure 1.3. Diagram representation of an indoor atmospheric chamber facility. Used to study aerosol formation and gas-to-particle kinetics. Gas analytes and oxidizers go into inlet and gas/particle mixture is collected for analysis through the outlet into the instruments. UV lights for photolysis, aerosol and gas-phase instrumentation, temperature and humidity control. Adapted from Ref. 52.

Thus, kinetic modeling of the mechanisms of atmospheric photooxidation of the gas-phase compounds being studied in the chamber experiments is used to develop reliable and accurate chemical models. These models will help have precise estimations and quantification of the impacts that aerosols can have in the atmosphere. They will help decipher the mechanisms by which different gas-phase volatile organic compounds interact to produce the wide range of aerosol particles observed in the atmosphere.[56] In this work, kinetic models for the atmospheric photooxidation mechanisms of DMDS, DMS and TMA

were developed and benchmarked against experimental data obtained from atmospheric chamber experiments of those compounds.

2 Instrumentation and Methods

Chamber experiments done by collaborators at UC Riverside to study the atmospheric photooxidation of sulfur and nitrogen containing compounds provided experimental data to guide the development and optimization of the kinetic models of the gas-phase atmospheric oxidation of DMDS, DMS and TMA presented here.

2.1 Atmospheric Chamber Facility

The atmospheric chamber facility in which the experiments were performed has a total volume of 37.5 m^{-3} and it is housed in an enclosed room with the following dimensions: 297.5in x 141.5in x 98.25in (LxWxH). The chamber is filled only with filtered air, which can be dry or with a certain level of relative humidity, but all the experiments presented use only dry air. 192 UV lamps induce photooxidation. Teflon® walls are used because it does not have significant absorbance in the wavelength range used to promote the photolytic reactions. This allows the light within the wavelength range needed for photooxidation of the organic compounds of interest through. Teflon® also has low absorptivity towards organic compounds used in these experiments, which helps minimize the loss of gas molecules due to condensation against the walls of the chamber. The instruments used to analyze the samples from the chamber include NO_x analyzer, CO analyzer, O_3 analyzer, selected ion flow tube mass spectroscopy (SIFT-MS), proton transfer reaction mass spectroscopy (PTR-MS), high resolution time of flight aerosol mass spectroscopy (HR-ToF-MS), scanning mobility particle analyzer (SMPS), hygroscopicity tandem differential mobility analyzer (TDMA), volatility TDMA, aerosol particle mass analyzer-SMPS, and an injection oven. Data from the SIFT-MS and gas-chromatography

instruments was used to develop and benchmark the kinetic models of DMDS, DMS and TMA.

2.1.1 Collection of Experimental Data

Due to the different rates at which the compounds being studied in the chamber experiments are photooxidized, the duration of the experiments differed from one to another. For the chamber experiment of DMDS for example, the data used to benchmark the model had 140 minutes of collected data with data points collected every 10 minutes with a Medor GC. This instrument uses a redox reaction with chromate as the oxidant, so it will not detect sulfur compounds in the 6+ oxidation state. The DMS experimental data was collected with the SIFT-MS and had 440 minutes. The SIFT-MS is a chemical ionization mass spectrometer that uses water as the reacting gas, so it detects compounds that will react with H_3O^+ to take a proton. The data for this experiment was collected in intervals of 10 minutes, with only 1 second in between each interval, and in each 10-minute interval data points collected every second within the 10 minutes. Lastly, the TMA experimental data counted with 453 minutes, and data points collected every 3 minutes from the SIFT-MS. The difference in duration and intervals between data points collected was selected depending on the photooxidation rates of the parent compounds, which vary due to their chemical properties and the sensitivity towards the black light emitted by the chamber's light sources. The experimental data collected using the SIFT-MS instrument expresses the number of ion counts for a given m/z peak of interest. Thus, to obtain quantitative data, a calibration through a SIM scan is necessary, this calibration was done for the DMS experimental data. However, for the experimental data used for the TMA kinetic modeling the SIFT-MS data is not calibrated, thus this data only shows quantitative

trends of an increase or decrease in the number of counts of any given m/z peak. In this data, if an increase or decrease of the number of counts by 20% is observed, it does correlate to an increase or decrease in concentration of the corresponding compound by 20%. However, this correlation applies to individual peaks, thus, a 20% decrease of one compound's peak is not necessarily a 20% decrease compared to another compound's concentration.

2.2 Kinetic Modeling

Kinetic modeling is a tool that allows to mathematically simulate the experimentally observed process of aerosol formation. This method allows to study the mechanisms in a more confined way by minimizing the uncertainties about the kinetics behind these processes due to the inability to isolate individual steps of the mechanisms during the experimental procedures. This method utilizes available information from experiments, such as mass to charge ratios and concentrations from mass spectroscopy analysis of gas-phase and aerosol species inside the chamber walls during the duration of the experiment. To produce a model that allows this data to be reproduced and give insights into the plausible mechanism that aerosol formation follows.[56] In this work, the kinetic models of atmospheric photooxidation of DMDS, DMS and TMA were benchmarked using the least squares method to compare the models' concentrations of the compounds of interest with data obtained from chamber experiments.

2.2.1 General Description and Previous Studies

The work previously done by Yin et al.[57] on developing mechanism for the atmospheric gas-phase oxidation of DMDS and DMS was used as the initial stage for developing the kinetic models of those two compounds. A scheme of the mechanistic

model for atmospheric oxidation of DMDS proposed by Yin et al. is shown in Scheme 2.1, where the most relevant products expected to be produced and the parent compound are shown in a box.

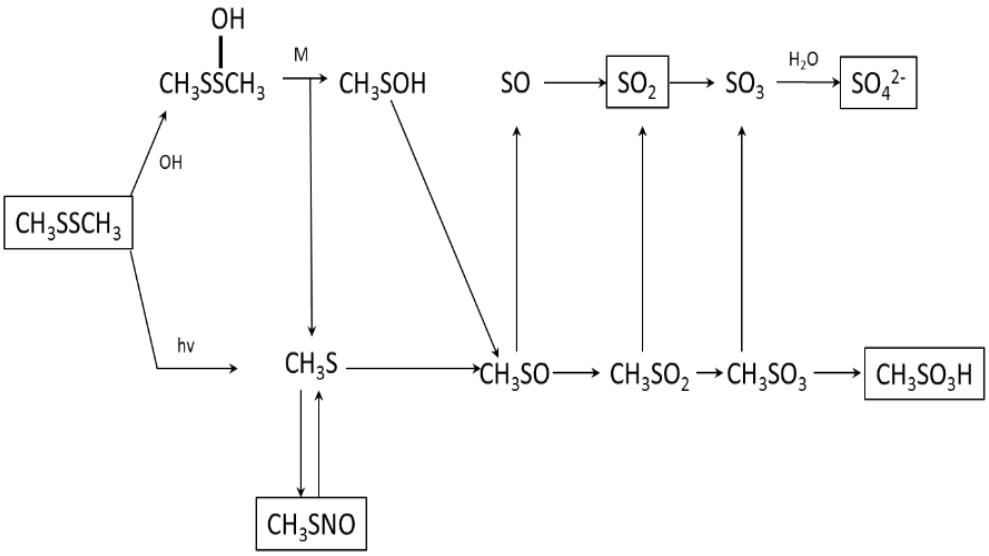

Scheme 2.1 DMDS Atmospheric Photooxidation Mechanism proposed by Yin et al. used to develop the kinetic model of DMDS being benchmarked in this work. Adapted from Ref. 57

The models gave satisfactory results for the gas-phase products of these processes, among which are SO_2, HCHO, H_2SO_4 and CH_3SO_3H. As can be observed from Scheme 2.1 the most relevant reactants considered by the model are the photooxidation of the parent compound, the addition of OH radical onto the parent compound, and then reactions and oxidation due to atmospheric species such as HO_2, O_2, and NO_x species.

Those same atmospheric oxidizers were considered to develop the kinetic model of DMDS and DMS here presented. Scheme 2.1 illustrates the two main pathways by which DMDS gets oxidized in atmosphere, which are photooxidation and OH-addition. Those two possible initial pathways might vary in relevance depending on the conditions of the atmosphere at a given time. From Scheme 2.1 it can be observed how with variations on

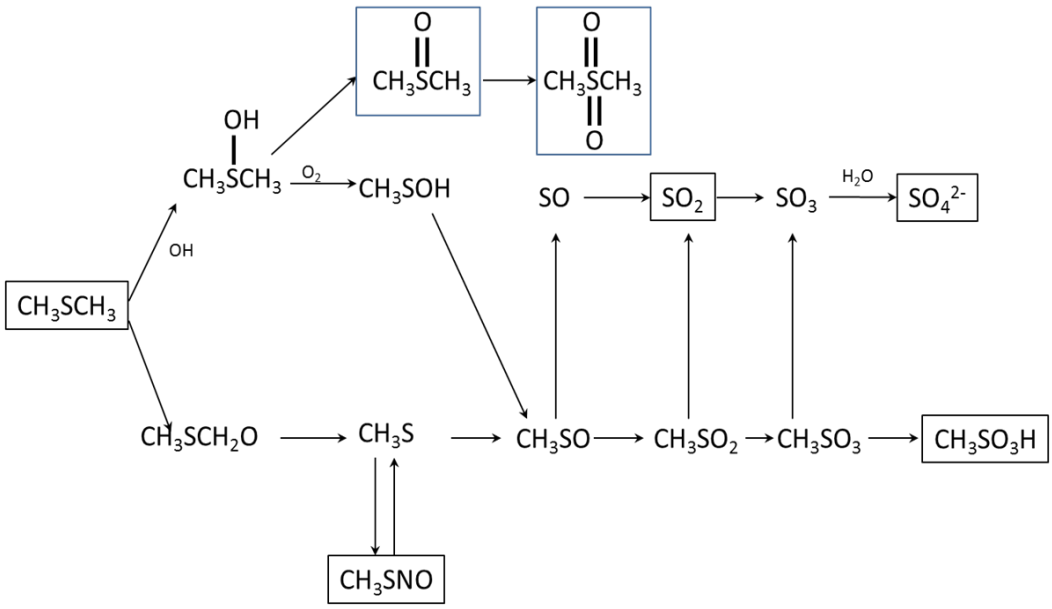

Scheme 2.2 DMS atmospheric photooxidation mechanism used to develop the DMS kinetic model being benchmarked in this work. Adapted from Ref. 57

the amounts of sunlight and OH radicals available in the atmosphere nearby any given DMDS source origin can dictate what would be more likely the preferred pathway by which DMDS gas molecules can be oxidized in the atmosphere. The same can be said for the atmospheric oxidation of DMS, as Scheme 2.2 also shows two possible pathways that the atmospheric oxidation of DMS can follow, depending on the concentrations of OH and NO_x species that are available near a DMS source. Although both mechanisms (DMDS and DMS) show most of the same compounds produced, Scheme 2.2, which represents the model for DMS, includes the formation of DMSO as one of the main products for this mechanism. Another difference between these two mechanisms is that one of the initial pathways by which the parent compound DMDS is oxidized is by direct photooxidation due to light ($h\upsilon$), while neither one of the two initial oxidative pathways suggested for DMS in Scheme 2.2 are dependent on the presence of oxidizer species OH and NO_x. This

suggests that for DMS, the photooxidative pathway is not dominant in atmospheric conditions, rather the OH-addition pathway is favored. Another commonality between the models for DMDS and DMS includes the formation and dissociation of CH_3SNO, which was considered to be a plausible trap towards the further oxidation of the gas-phase sulfur that could prevent or hindrance the formation of SO_2. This trap is potentially important for experiments in which amines are oxidized as that would provide higher concentrations of NO_x. The kinetic model for the atmospheric oxidation of TMA was guided by previous studies of different amines. The starting baseline for the development of a model for this compound can be seen in Scheme 2.3. The model, proposed by Nielsen et al.[49], propositions $(CH_3)_2NCHO$, CH_3NCH_2, $(CH_3)_2NNO_2$, HCHO, and $(CH_3)_2NNO$ as the major products for the atmospheric oxidation of TMA. This mechanism, like the one for DMS, only considers the oxidation of the parent compound through interactions with radical species present in the atmosphere, specifically OH radicals. These three initial models were used to build the kinetic models presented in this work. Additional reactions and optimizations

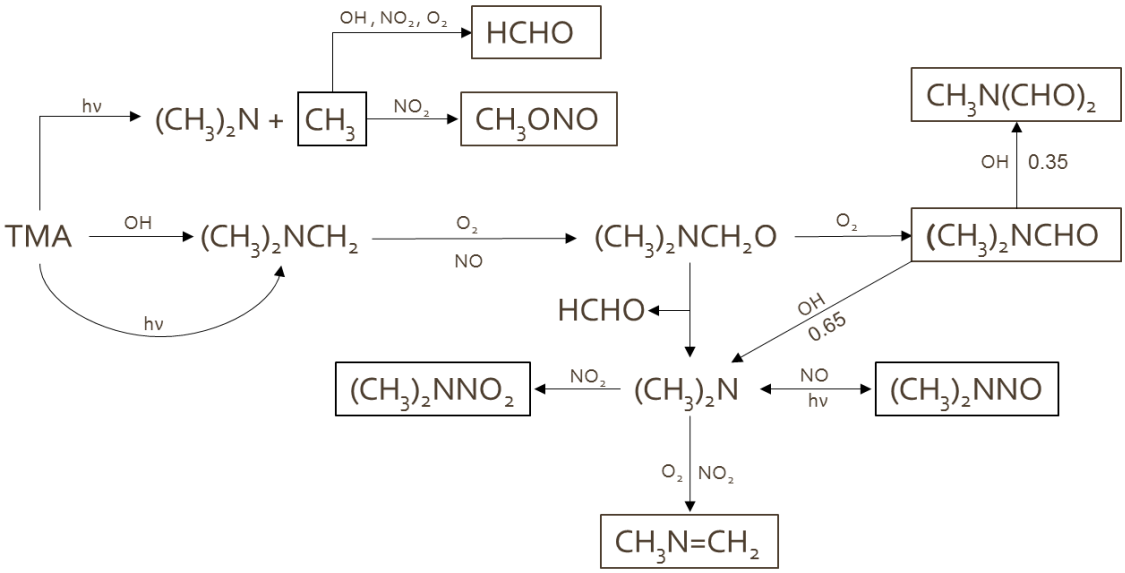

Scheme 2.3. TMA atmospheric photooxidation mechanism. Scheme of reaction mechanism used to develop the TMA kinetic model benchmarked being benchmarked in this work. Adapted from Ref. 49

of some of the proposed rate constants were performed to obtain better agreement to the experimental data produced by collaborator

2.2.2 Inclusion of Varying Concentrations of Oxidizers

One of the first additions made to the kinetic models was to introduce a variable term for the initial concentrations of the oxidizer species. Then reactions that those oxidizer sources follow in the atmosphere to produce compounds were included. This was implemented because the atmospheric chamber experiments utilized H_2O_2 and N_2O_5 as the initial sources for OH and NO_x species to promote oxidation of the parent compounds. Inclusion of these reactions in the mechanism allows to more accurately monitor the formation of those compounds and their consumption as they partake in the oxidation of gas-phase molecules and the formation of aerosol particles. Table 2.1 shows the reactions that were included in the mechanisms for this purpose, along with the rate constants used for each reaction.

Table 2.1 N_2O_5 and H_2O_2 Dissociation Reactions and Respective Rate Constants Included in Kinetic Models.

$\boldsymbol{N_2O_5 \rightarrow NO_2 + NO_3}$	$k = 5.2x10^{-2}$
$\boldsymbol{NO_2 + NO_3 \rightarrow N_2O_5}$	$k = 1.2x10^{-12}$
$\boldsymbol{NO_3 \overset{M}{\rightarrow} NO + O_2}$	$k = 3.0x10^{-3}$
$\boldsymbol{NO_3 \overset{M}{\rightarrow} 0.3NO + 0.7NO_2 + 0.7O(^3P)}$	$k = 1.55x10^{1}\, k_{NO_2}$
$\boldsymbol{H_2O_2 \overset{hv}{\rightarrow} 2OH}$	$k = 7.1x10^{-4} k_{NO_2}$

2.2.3 Inclusion of Photolysis and Wall Loss Rates

Because the facility in which chamber experiments are performed can affect the observed results by providing the contents inside the chamber's walls with different light flux or wavelengths. A term for the specific photolysis rate that is specific to the conditions

of the chamber facility where the experiments were performed was included in the kinetic models. This is advantageous because it allows the model to simulate experimental data under different photolytic conditions, and it because several of the reactions included in the mechanisms are dependent on the photolysis rates, it allows to more accurately represent the oxidation process. The chamber's NO_2 photolysis rate as reported by Cocker et al.[52] of 0.025 s^{-1} was used for the kinetic models. Another way that atmospheric chambers might influence the results of an experiment is due to the adsorption of gas-phase molecules onto the surface of the Teflon® walls of the chamber.[57] However, no evidence of any amine or reduced sulfur gas phase losses to the Teflon® wall surface has been seen on the collection of the experimental data. This occurrence leads to the addition of gas-to-wall reaction rates with values of 0 s^{-2} for the parent compounds DMDS and DMS, as well as the product of SO_2.

2.2.4 Kinetic Modeling Configurations

The code for the kinetic models was developed using *Mathematica* 11 software from Wolfram.[58] This platform offers a practical interface that utilizes the Wolfram Language's wide variety of tools. The Wolfram language provides special functions and algorithms to find numerical or symbolic solutions for different kinds of differential equations, such as those describing the change in concentration over time of the compounds included in the kinetic models. This feature allows interpretation of functions to represent solutions in forms that can be immediately manipulated or visualized. An example of a differential equation 1, $\boldsymbol{d[N_2O_5] = -k_{N1}[N_2O_5] + k_{N2}[NO_3][NO_3]dt}$ shows one of the equations utilized in the models to evaluate the change in concentration of N_2O_5 as it breaks down into other NO_x species. From this equation, it can be observed that the $[N_2O_5]$

concentration term depends on the reaction rates k_{N1} and k_{N2}, and by the [NO_3] concentration term over the independent variable time (t). As the example from Eq.1 shows, the concentrations of N_2O_5 and NO_3 are dependent on each other, but it is possible to write a system of equations which would describe the change in concentration over time of both compounds to evaluate them. For this, a second equation describing the change of [NO_3] over *dt* would be necessary, and like this example, the same principle was used to develop the kinetic models presented in this work. The models are composed of a system of differential equations which ties together the interconnections of the changing concentrations of each of the compounds involved in the model.

2.2.4.1 System of Differential Equations Solver

The systems of differential equations representing each of the kinetic models represented here were evaluated using the NDSolve function from the Wolfram Mathematica Software.[58] NDSolve is a built-in function of the software that allows to solve for many types of differential equations, such as ordinary or partial differential equations. The method used by NDSolve depends on the type of the equation(s) being solved. The available methods NDSolve can use include the explicit and implicit Euler and explicit and implicit Midpoint methods. NDsolve gives the results for the equations in term of 'Interpolating function' objects, which represent a function whose values are found by interpolation, and these functions represent the solutions to each equation of the system. Although there are many possible configurations available to use with the NDSolve function, in this work, the format used for this work had the form **NDSolve[{*eqn1, eqn2,…}, {y1, y2, …}, {x, x_{min} , x_{max} }*]** which finds numerical solutions for each '***eqn***', while each ***eqn*** represent a ***y*** term with the independent variable ***x*** in the range x_{min} to x_{max}.

In this set-up, each of the ***y***'s represent a dependent variable, which in this case would be the concentration of each the chemical compounds involved in the model, where ***x*** represents the independent variable time, in the range from the starting experimental time, x_{min}, (taken to be 0 min) and the end experimental time x_{max}. With this setup the NDSolve function gives solutions for the derivatives of ***y*** with respect to ***x***, *or* ***y[x]*** rather than for the function itself. This allows evaluation and monitoring of the changes in concentration over time based on the model's system of equations, allowing one to optimize the parameters of the mechanisms.

2.2.4.2 Step Size and Number of Steps

The Mathematica software allows varying the configurations of the NDSolve function, and among these configurations are the maximum number of steps that the evaluation of the kinetic model's system of differential equations is to take to reach a solution. This was configured for the evaluation of the kinetic models presented in this work using the command "MaxSteps". This command of "MaxSteps" allows the option of having an unlimited number of steps to complete an evaluation by using the command 'MaxSteps → *infinity*', which ensures the calculation for a solution is not terminated before reaching a solution.[58] This configuration was used in every evaluation of the kinetic models to ensure the best solutions to the equations were found without truncating the evaluations of the model. The size of the steps, or the size of the time lapse, "dt", of each step was kept constant throughout all the evaluations at 1. Thus, the step size of the evaluations was kept at a maximum of 1 minute.

2.2.4.3 Parameter Optimization

After the script and system of ordinary differential equations of the kinetic model was in place and the initial values for the concentrations of the compounds in the model agree with experimental initial concentrations, the values of several rate constants needed to be optimized to ensure the best fit possible to the experimental data available. The optimization of parameters like rate constants and initial concentrations was done utilizing Mathematica's built-in symbol "**For**" in combination with the least squares method.[58] The "**For**" symbol has the form "**For[*start, test, incr, body]"*** and it evaluates its arguments in a non-standard way by repeatedly evaluating the "***body***", which is the argument of interest for the optimization of a given term, from the starting condition "***start***", and increasing that initial condition in increments by "***incr***" until "***test***" fails to be true. In this work the "**For*"*** function was used to systematically evaluate multiple sets of values for the rate coefficients that needed to be optimized in each of the kinetic models.

Then, to evaluate the accuracy with which a given set of values represented the experimental data against which the kinetic model was being benchmarked, the least squares method was used to compare the modeled and experimental data. The least squares method is described by the equation $\boldsymbol{S = \sum_{i=1}^{n} (r_i)^2}$, where the sum of all the individual r_i is squared to give the total least squares value, "**S**". From the least squares equation, each individual r_i term represents a compound that is being compared to experimental data, and the r_i term is defined as $\boldsymbol{r_i = y_i - f(x_i, \beta)}$. Where y_i is the experimental data points at their specific times and the $f(x_i, \beta)$ represents the modeled data points according to the function describing the model at the same specific times as those of the experimental data. Thus, the total least squares residual would be from all the compounds of which

experimental data is available to benchmark. Then, the lower the "**S**" value, the closer fit to the experimental data the model reaches.

3 Kinetic Models and Benchmarking

The DMDS, DMS and TMA kinetic models were benchmarked against the compounds with experimental data available to ensure the models could replicate the results from atmospheric chamber experiments. This process was done by individually comparing the concentrations of the experimental and the modeled data at the specific times at which the experimental data were collected for each of the compounds that experimental data was available, which includes DMDS and SO_2 for the DMDS model. Only experimental data for the gas-phase photooxidation of DMS was benchmarked for the DMS model, while for the TMA model the compounds with experimental data available were trimethylamine, N-dimethylformamide, N-methylmethanimine, formaldehyde, and nitromethane. The experimental and modeled data were compared to one another using least squares method to evaluate which values of the incorporated rate constants would better satisfy the observed experimental data. Among those values are gas-to-aerosol rates for DMDS and DMS models and the rate constants of 6 of the reactions included in TMA model.

3.1 DMDS Kinetic Model

The kinetic model for the atmospheric oxidation of DMDS developed for this work counts with 46 reactions. Table 3.1 shows the reactions that were included in this model and the rate constants correspondent to each reaction of the mechanism including those accounting for gas-to-wall effects for SO_2 and DMDS in Reactions 27 and 28 and the dissociation reaction of H_2O_2 into OH radicals in Reaction 23. The reactions for the dissociation of N_2O_5 and formation of NO_x species were also included in the model but are not counted as part of the DMDS atmospheric oxidation mechanism, and thus they are not explicitly included

in Table 3.1 or any of the tables including the reactions of each of the kinetic models (Tables 3.1 – 3.3). The reactions included in this model are for the gas-phase mechanism of atmospheric oxidation of DMDS, and with exception of the reactions that account for the wall effects of the chamber, they do not explicitly account for the formation of aerosol particles under atmospheric conditions such as the ones under which the chamber experiments were performed. The mechanism represented by these reactions show two pathways of parent compound oxidation. The first is in reaction 1, which shows the OH-addition pathway. The second is in Reaction 21 which shows the photooxidative splitting of the disulfide bond (S-S) of DMDS. The photooxidative splitting of the S-S bond results into two equal radical molecules of CH_3S, which can undergo a reverse reaction to form again the parent compound, as shown in Reaction 22, however this reverse reaction occurs at a much slower rate at the partial pressures in the chamber.

Table 3.1 Reactions in DMDS Model and respective rate constants. Adapted from Ref 29. [57]

	Reaction	Rate Constant, k[a]
1.	$CH_3SSCH_3 + OH \rightarrow CH_3SOH + CH_3S$	$k = 2.41x10^{-10}$
2.	$CH_3SOH + OH \rightarrow CH_3SO + H_2O$	$k = 1.1x10^{-10}$
3.	$CH_3S + O_2 \rightarrow CH_3SOO$	$k = 5.8x10^{-17}$
4.	$CH_3S + O_2 \rightarrow CH_3 + SO_2$	$k = 5.94x10^{-17}$
5.	$CH_3S + O_3 \rightarrow CH_3SO + O_2$	$k = 6.0x10^{-12}$
6.	$CH_3S + CH_3SOO \rightarrow 2\,CH_3SO$	$k = 8.0x10^{-11}$
7.	$CH_3SO \rightarrow CH_3 + SO$	$k = 5.0x10^{-5}$
8.	$CH_3SO + O_2 \rightarrow CH_3SOOO$	$k = 7.7x10^{-18}$
9.	$SO + OH \overset{O_2}{\rightarrow} SO_2 + HO_2$	$k = 1.1x10^{-10}$
10.	$SO + O_3 \rightarrow SO_2 + O_2$	$k = 8.9x10^{-14}$
11.	$SO + O_2 \rightarrow SO_2 + O\cdot$	$k = 6.7x10^{-17}$
12.	$CH_3SO + O_3 \rightarrow CH_3SOO + O_2$	$k = 2.0x10^{-12}$
13.	$CH_3SOH + CH_3SO_3 \rightarrow CH_3SO_3H + CH_3SO$	$k = 3.4x10^{-12}$
14.	$CH_3SOOO + CH_3S \rightarrow CH_3SOO + CH_3SO$	$k = 7.0x10^{-11}$
15.	$CH_3SOO \rightarrow CH_3 + SO_2$	$k = 1.1x10^{1}$

Table 3.1 Continued - Reactions in DMDS model and respective rate constants

Reaction	Rate Constant, k[a]
16. $CH_3SO_3 + H^+ \rightarrow CH_3SO_3H$	$k = 1.1x10^{-4}$
17. $CH_3SOO + O_3 \rightarrow CH_3SO_3 + O_2$	$k = 5.0x10^{-15}$
18. $CH_3SOO + O_2 \rightarrow CH_3SO_4$	$k = 2.6x10^{-18}$
19. $CH_3SOO \rightarrow O_2 + CH_3S$	$k = 6.0x10^{2}$
20. $CH_3SOO + OH \rightarrow CH_3SO_3H$	$k = 5.0x10^{-11}$
21. $CH_3SSCH_3 \xrightarrow{hv} CH_3S + CH_3S$	$k = 5.0x10^{-3}k_{NO_2}$
22. $CH_3S + CH_3S \rightarrow CH_3SSCH_3$	$k = 4.15x10^{-11}$
23. $H_2O_2 \xrightarrow{hv} 2\ OH$	$k = 7.1x10^{-4}k_{NO_2}$
24. $SO_2 + OH \xrightarrow{M} HOSO_2$	$k = 1.1x10^{-12}$
25. $HOSO_2 + O_2 \rightarrow HO_2 + SO_3$	$k = 4.0x10^{-13}$
26. $HOSO_2 + OH \rightarrow H_2SO_4$	$k = 1.0x10^{-11}$
27. $CH_3SSCH_3 \rightarrow Wall$	$k = 0.0$
28. $SO_2 \rightarrow Wall$	$k = 0.0$
31. $CH_3SOOO + CH_3SO \rightarrow CH_3SO_2 + CH_3SO_2$	$k = 8.1x10^{-12}$
32. $CH_3SO_3 + H_2O_2 \rightarrow CH_3SO_3H + HO_2$	$k = 3.0x10^{-16}$
33. $CH_3SOOO + CH_3SOOO \rightarrow 2\ CH_3SO_2 + O_2$	$k = 6.0x10^{-12}$
34. $CH_3SOOO \rightarrow CH_3SO + O_2$	$k = 1.7x10^{2}$
35. $CH_3SO + OH \xrightarrow{M} CH_3SO_2H$	$k = 5.0x10^{-11}$
36. $CH_3SOH + OH \rightarrow CH_3SO_2 + H_2O$	$k = 1.6x10^{-11}$
37. $CH_3SO_3 \rightarrow CH_3 + SO_3$	$k = 1.6x10^{-1}$
38. $CH_3S + NO_2 \rightarrow CH_3SO + NO$	$k = 6.1x10^{-11}$
39. $CH_3SOO + NO \rightarrow CH_3SO + NO_2$	$k = 1.4x10^{-11}$
40. $CH_3SO + NO_2 \rightarrow CH_3SO_2 + NO$	$k = 3.0x10^{-12}$
41. $CH_3SOOO + NO \rightarrow CH_3SO_2 + NO_2$	$k = 8.0x10^{-12}$
42. $CH_3SO_2 + NO_2 \rightarrow CH_3SO_3 + NO$	$k = 1.0x10^{-14}$
43. $CH_3SO_4 + NO \rightarrow CH_3SO_3 + NO_2$	$k = 1.0x10^{-11}$
44. $SO + NO_2 \rightarrow SO_2 + NO$	$k = 1.4x10^{-11}$
45. $CH_3S + NO \rightarrow CH_3SNO$	$k = 2.87x10^{-11}$
46. $CH_3SNO \xrightarrow{hv} CH_3S + NO$	$k = 0.5\ k_{NO_2}$
47. $CH_3SSCH_3 \rightarrow Aerosol$	$k = 0.58x10^{-4}\ s^{-1}$*
48. $SO_2 \rightarrow Aerosol$	$k = 1.81x10^{-4}\ s^{-1}$*

*Rates that were optimized in this work. [a]Rate constants are in units of molecules, cm^3 and sec.

3.1.1 DMDS Benchmarking

The gas-phase experimental data of a chamber experiment of DMDS reacted with H_2O_2 and UV lights on collected using Medor GC was used to benchmark the DMDS kinetic model. The data includes three calibrated sets of data points corresponding to a different compound each: one data set for the decreasing concentration of the parent compound DMDS, another one for the concentration of SO_2 being formed over time, and the third one for a compound of unknown identity. The third set was thought to be a possible precursor of methanesulfonic acid (MSA) from chamber experiment analysis. Because the identity of the third compound was uncertain, the model was only benchmarked using the experimental data for DMDS and SO_2. As shown in Figure 3.1, the experimental data had an initial concentration of 42.6 ppb of DMDS and about 1.93 ppb for SO_2. These initial concentrations were used for the kinetic model optimization. In Figure 3.1 an increase in concentration of SO_2 from 1.93 to 22.3 ppb can be observed,

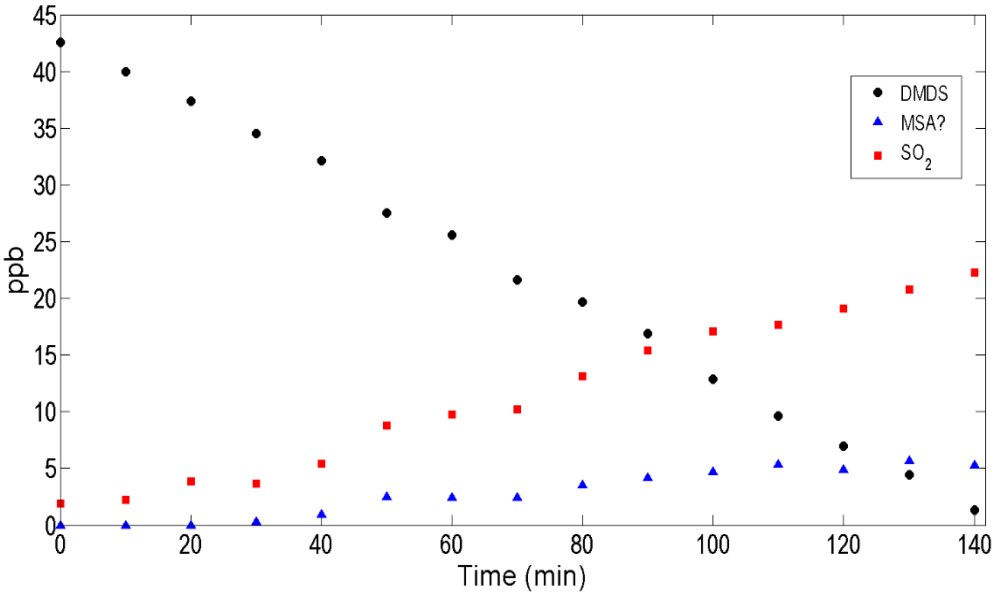

Figure 3.1 Concentration as a function of time of DMDS, SO_2, and unknown obtained from GC-MS from atmospheric chamber experiment. This is the set of experimental data used to benchmark the kinetic model for atmospheric oxidation of DMDS developed in this work.

while the concentration of DMDS decreases from its initial of 42.6 to 1.33 ppb; and the third set of data points also shows an increase in concentration, from 0 to 5.3 ppb. This means that roughly half of the starting gas-phase DMDS is photooxidized and forms SO_2 in the gas-phase, while the other half of its initial concentrations either goes into forming other gas-phase products, such as MSA, or it goes into forming aerosol particles, which are not detected by the gas-phase instrumentation. Thus, for this kinetic model it was important to address how much of the gaseous sulfur was contributing towards the formation of aerosol particles and what effects that might have on the overall gas-phase atmospheric photooxidation mechanism of DMDS. The focus on the first stage of this study was to compare the previously proposed reaction rates from the work by Yin et al. for the atmospheric photooxidation of DMDS to gas-phase experiments from the atmospheric chamber to observe the accuracy with which this kinetic model represented the experimental data. At this stage, the emphasis was on the oxidation of DMDS and the production of SO_2 due to its known readily atmospheric oxidation into aqueous sulfate ions and role as SOA seed.

3.1.2 Formation of SO_2 and Oxidation DMDS

First, the kinetic model described by the reactions in Table 3.1 was evaluated using the same initial concentrations for DMDS and oxidizers as the experimental data obtained from chamber experiments described in Section 3.1. The data from the evaluation of the kinetic model compared to the experimental data from chamber experiments is shown in Figure 3.2. From this experiment, the objective was to look at the kinetic model's ability to simulate the oxidation of DMDS and formation of SO_2 without optimization of the reaction rates or adding any gas-to-aerosol reactions to the model from Table 3.1. Figure

3.2 shows the change in concentrations over time of the compounds DMDS and SO_2 from both experimental and kinetic model are compared. The DMDS and SO_2 kinetic model data is presented with black and red solid lines respectively and experimental data is presented in black and red markers. The model as well as the experimental data show a decay of the parent compound (DMDS) and the production of oxidation products. The most abundant product formed from DMDS oxidation is SO_2, this compound is formed in a concentration of more than 40 ppb according to the modeled data, as seen in Figure 3.2. Without the addition of gas-to-aerosol rates to the model, the comparison of data from the DMDS kinetic model and the experimental data showed a large discrepancy on the concentrations of SO_2 and DMDS due to fact that the model only accounts for gas-phase oxidation reactions. Not accounting for the formation of aerosol particles in the kinetic model led to the model to predict an excess of 20 ppb of SO2 and 13 ppb of DMDS, due to the uptake of gas-phase molecules into aerosols not being modeled in the mechanism.

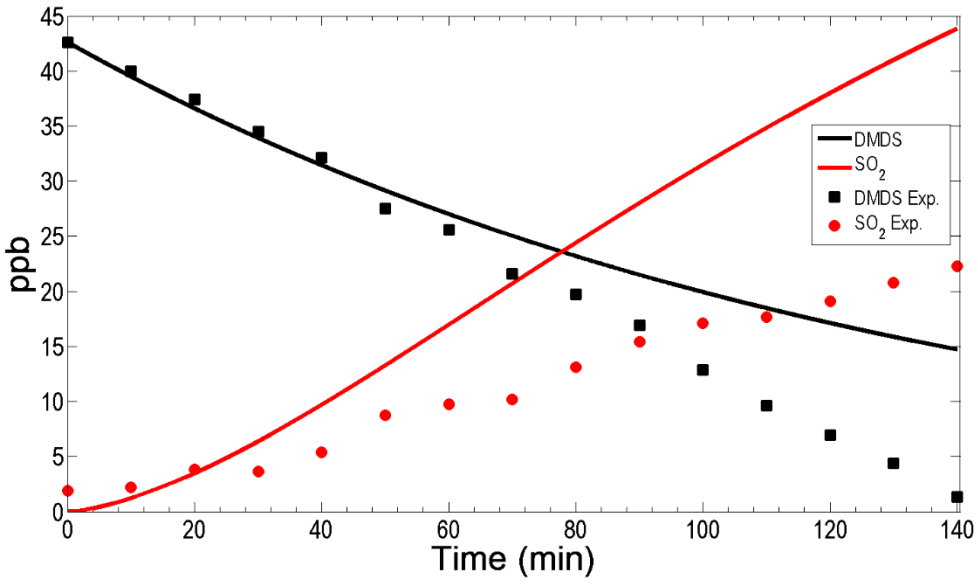

Figure 3.2. Comparison of DMDS and SO_2 concentrations as a function of time of modeled and experimental data. Aerosol formation rates for both species are set to zero, and the solid lines represent the data from the model while the markers show the experimental data.

This observation is in agreement with atmospheric chamber experiments where the oxidation of the initial parent species by chemical and photolytic induced pathways leads to the formation of aerosol particles. The particles encapsulate a percentage of the oxidized gas-phase products and takes them out of the gas-phase and into the aerosol phase. The aerosol particles also prevent some of the oxidized gas species from being perceived by the instrument and thus leads to a discrepancy observed between the experimental and modeled data in Figure 3.2.

3.1.3 Gas-to-aerosol Optimized Rates of SO_2 and DMDS

After comparing the initially proposed model in the first stage of the study, the second stage required to make the model more accurately represent the gas-phase experimental data. For this, a rate of gas-to-aerosol formation for each DMDS and SO_2 was included into the model and optimized to achieve the best possible fit whilst keeping the rest of the rates the same. In doing this, the concentrations of the gas-phase species DMDS and SO_2 became a drastically better fit to the experimentally observed concentrations, as observed in Figure 3.3. The optimized values for the gas-to-aerosol rates are 0.58×10^{-4} s^{-1} for DMDS-to-aerosol and 1.81×10^{-4} s^{-1} for SO_2-to-aerosol, these rates gave the lowest possible least squares values (**S**), which were 207.521 and 57.4076 for DMDS and SO_2 respectively. The optimized gas-to-aerosol rates are pseudo-first order and were incorporated to analyze the amounts of sulfur that ought to be found in the aerosol particles that are formed during the chamber experiments. The optimized gas-to-aerosol rates are likely to reduce the error from estimations of sulfur content in aerosols. In Figure 3.3, the production of SO_2 from the model is in agreement with experimental data, and the implementation of the gas-to-aerosol rates gives a more reliable way for modeling

concentrations of atmospheric chamber experiments and with more studies may lead to more accurate global chemical transport models that will be able to better simulate climate.

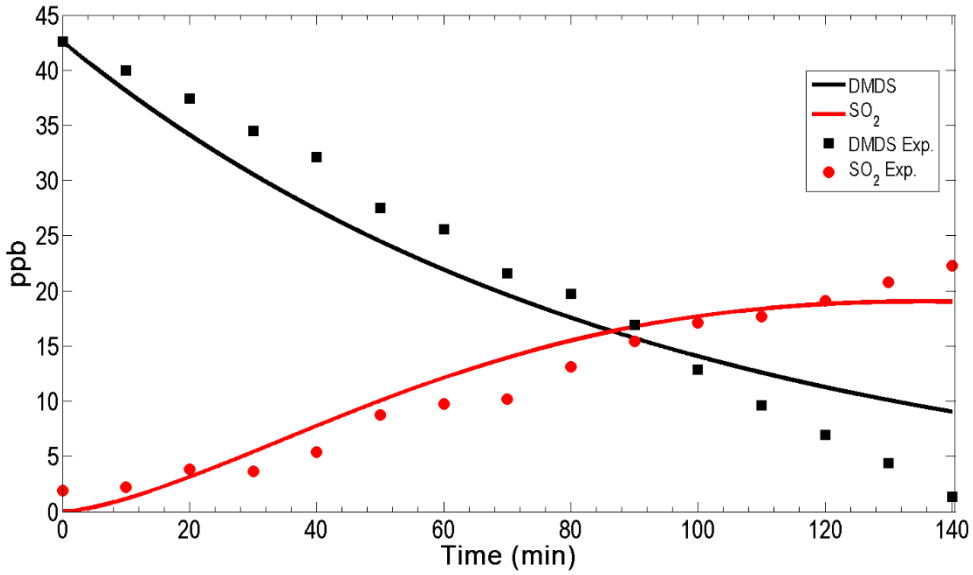

Figure 3.3. Comparison of DMDS and SO_2 concentrations as a function time of modeled and GC-MS data with the optimized gas-to-aerosol rates. Aerosol formation rates for both species were optimized. Solid lines represent the data from the model and the markers show the GC-MS data.

However, the formation of other by-products from the oxidation of DMDS is of relevance as well. Thus after benchmarking the SO_2 and DMDS concentrations of the model, looking into what other chemical species might be produced in high concetrations or might be of relevance to aerosol formation was the next step.

3.1.4 Modeled Concentrations of MSA, CH_3S, and CH_3SO

Apart from SO_2 , other radicals and by-products such as methanesulfonic acid are also expected to be produced from the oxidative mechansim in Scheme 2.1. Although, no experimental data from the atmospheric chamber was available for these compounds, to look at their concentrations according to the kinetic model is insightful to provide

qualitative undestanding of the atmospheric oxidation process of DMDS. Figure 3.4 shows the change in concentration over time of the chemical species that were included in the model and were simulated to have the highest concentraions including DMDS and SO_2. In Figure 3.4 the concentration of the CH_3SO radical increases until 3400 s then plateaus and decreases.

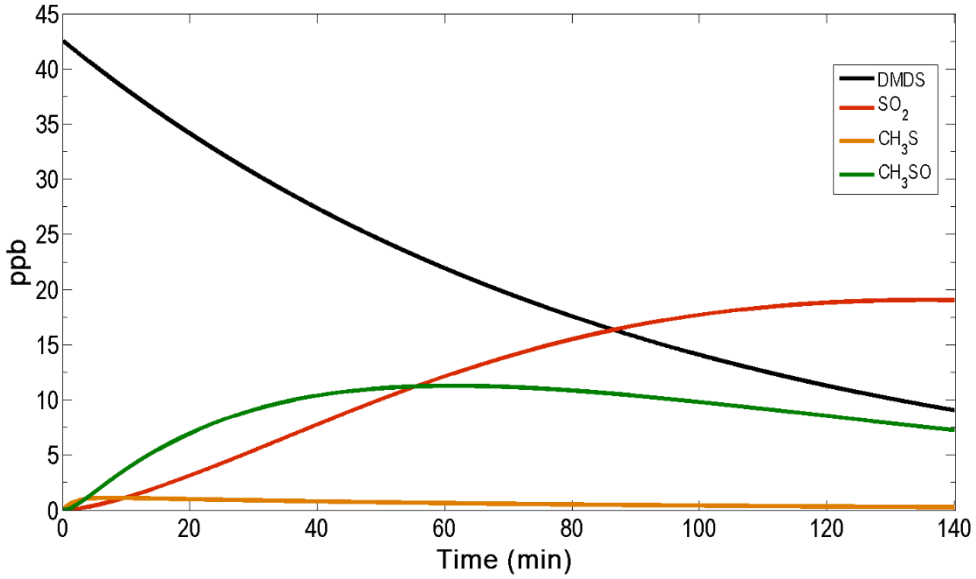

Figure 3.4. Concentration as a function of time of compounds from DMDS atmospheric oxidation model. of DMDS, SO_2 and $CH_3S^{\cdot}$ and $CH_3SO^{\cdot}$ radical species; by-products of higher concentrations.

At 3400 s, the concentrations of SO_2 and CH_3SO are the same and then SO_2 concentration continues to increase while at that point the CH_3SO concentration starts to decrease, which might indicate a correlation as CH_3SO is oxidized and SO_2 is being formed. Although SO_2 is of great enviromental concern when it comes to organosulfur compouds, other sulfur containing compounds might have the opportunity to become of greater impact as measures are taken to supress the emissions of SO_2.[3] For this reason, MSA is also a compound of interest when studying the atmospheric oxidation of DMDS, as it has been

observed by other research groups during laboratory experiments that MSA contributes greatly towards the formation of aerosol particles when water and low-volatility amine comounds are present.[48] Although MSA has been shown to enhance the formation of aerosols under these conditions, the concentrations at which it is produced in these chamber experiments might not be of great concern.

Figure 3.5 shows the modeled concentrations from the atmospheric oxidation of DMDS model of MSA and of the radical species CH_3SO_3. The modeled highest concentration of MSA from the atmospheric photooxidation of 42.6 ppb of DMDS is merely 0.79×10^{-11} ppb, which is negligible compared the near to the 21 ppb of SO_2 produced. By comparison, the concentration of MSA is irrelevant according to the modeled data. However, it is not consistent with experimental findings of other research groups, as field observations and well as atmospheric chamber experiments have found levels of atmospheric gas-phase MSA concentrations are typically in the range of $\sim10^5$–10^7

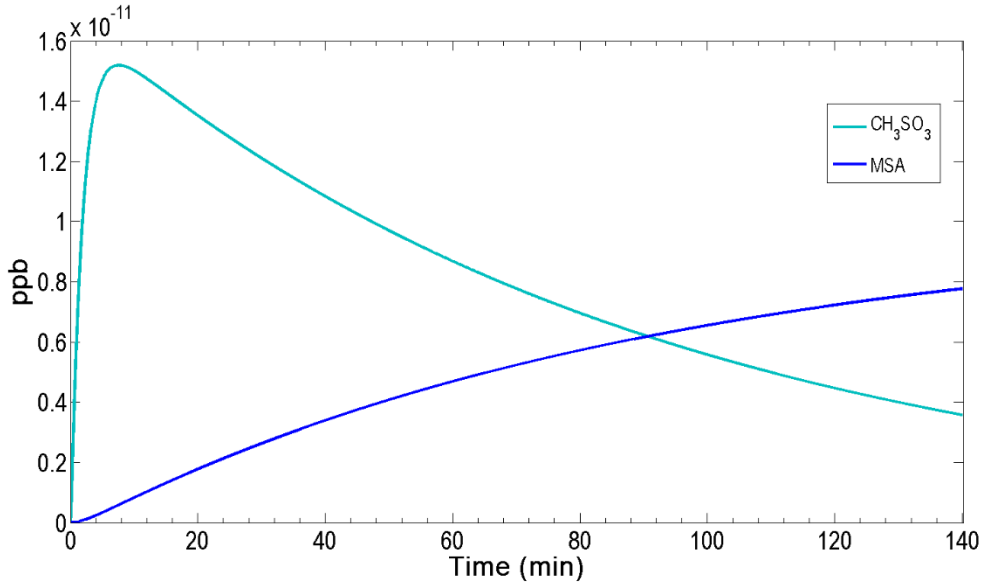

Figure 3.5. Concentration as a function of time of methanesulfonic acid (MSA) and CH_3SO_3 radical. Obtained from the DMDS atmospheric oxidation model.

molecules cm^{-3}, about ~10−100% of those of H_2SO_4.[51] Based on this range, the model predicts merely ~3.6×10^{-11} % of that of the SO_2 concentration. Thus, the model achieves a great agreement with the simulation of SO_2 and DMDS concentrations. However, more experimental data of MSA to compare to the modeled concentrations and further investigate the rates of formation of this compound is needed.

3.2 DMS Kinetic Model

After benchmarking of the kinetic model of DMDS the next stage of this study was to analyze the gas-phase atmospheric oxidation mechanism of DMS. DMS is a reduced-sulfur compound that is readily released into the atmosphere from marine phytoplankton and other sources such as farm waste. The reactions that were included in the kinetic model for DMS are presented in Table 3.2, including the gas-to-wall interactions in Reactions 52 and 53 and the dissociation reaction of H_2O_2 into OH radicals in Reaction 54. Although the reactions for the dissociation of N_2O_5 and formation of NO_x species were also included in the model they are not explicitly included in Table 3.2, instead they are shown in Table 2.1. The reactions included in this model are for the gas-phase mechanism of atmospheric oxidation of DMS and they do not explicitly account for the formation of aerosol particles from the chamber experiments. Reactions that account for the wall effects of the chamber are also included. The mechanism shows two main pathways of parent compound oxidation, the first one shown in Reactions 1 and 3 consisting on OH-addition followed by CH_3-dissociation. The second is shown in Reaction 2, consisting on H-abstraction from one of the CH_3 groups of DMS (CH_3SCH_3) by an OH radical. Both of these initial pathways of oxidation of DMS are mainly dependent on the amount of OH radicals present, thus the photooxidative pathway observed in DMDS is not as prominent for DMS.

Table 3.2. Reactions in DMS Model and respective rate constants. Adapted from Ref 57. [57]

Reaction	Rate Constant, k[a]
1. $CH_3SCH_3 + OH \rightarrow CH_3S(OH)CH_3$	$k = 1.7x10^{-12}$
2. $CH_3SCH_3 + OH \rightarrow CH_3SCH_2 + H_2O$	$k = 4.4x10^{-12}$
3. $CH_3S(OH)CH_3 \rightarrow CH_3SOH + CH_3$	$k = 5.0x10^{3}$
4. $CH_3S(OH)CH_3 + O_2 \rightarrow CH_3S(O)CH_3 + HO_2$	$k = 2.0x10^{-12}$
5. $CH_3S(O)CH_3 + OH \rightarrow CH_3S(O)(OH)CH_3$	$k = 5.8x10^{-11}$
6. $CH_3SCH_2 + O_2 \rightarrow CH_3SCH_2OO$	$k = 7.3x10^{-13}$
7. $CH_3SCH_2OO + NO \rightarrow CH_3SCH_2O + NO_2$	$k = 8.0x10^{-12}$
8. $CH_3SCH_2O \rightarrow CH_3S + HCHO$	$k = 1.0x10^{1}$
9. $CH_3S + O_2 \rightarrow CH_3SOO$	$k = 5.8x10^{-17}$
10. $CH_3SOO \rightarrow CH_3S + O_2$	$k = 6.0x10^{2}$
11. $CH_3S + O_3 \rightarrow CH_3SO + O_2$	$k = 6.0x10^{-12}$
12. $CH_3S + OH \rightarrow CH_3SOH$	$k = 5.0x10^{-11}$
13. $CH_3 + SO_2 \rightarrow CH_3SO_2$	$k = 2.9x10^{-13}$
14. $CH_3SO \rightarrow CH_3 + SO$	$k = 5.0x10^{-5}$
15. $CH_3SO_2 \rightarrow CH_3 + SO_2$	$k = 1.1x10^{1}$
16. $CH_3SOO + CH_3S \rightarrow CH_3SO + CH_3SO$	$k = 8.0x10^{-11}$
17. $CH_3SOO + NO \rightarrow CH_3SO + NO_2$	$k = 1.4x10^{-11}$
18. $CH_3S + NO_2 \rightarrow CH_3SO + NO$	$k = 6.1x10^{-11}$
19. $CH_3S + HO_2 \rightarrow CH_3SO + HO$	$k = 3.0x10^{-16}$
20. $CH_3SO + O_2 \rightarrow CH_3S(O)OO$	$k = 7.7x10^{-18}$
21. $CH_3S(O)OO \rightarrow CH_3SO + O_2$	$k = 1.4x10^{-2}$
22. $SO + NO_2 \rightarrow SO_2 + NO$	$k = 1.4x10^{-11}$
23. $SO + O_2 \rightarrow SO_2 + O^{\cdot}$	$k = 6.7x10^{-17}$
24. $SO + O_3 \rightarrow SO_2 + O_2$	$k = 8.9x10^{-14}$
25. $CH_3SO_2 + NO_2 \rightarrow CH_3SO_3 + NO$	$k = 1.0x10^{-14}$
26. $CH_3SO_2 + O_3 \rightarrow CH_3SO_3 + O_2$	$k = 5.0x10^{-15}$
27. $CH_3SO_2 + HO_2 \rightarrow CH_3SO_3 + OH$	$k = 2.5x10^{-13}$
28. $CH_3SO_2 + CH_3SO_2 \rightarrow CH_3SO_3 + CH_3SO$	$k = 7.5x10^{-12}$
29. $CH_3SO_3 \rightarrow CH_3 + SO_3$	$k = 1.6x10^{-1}$
30. $CH_3SO + NO_2 \rightarrow CH_3SO_2 + NO$	$k = 3.0x10^{-12}$
31. $CH_3SO + O_3 \rightarrow CH_3SO_2 + O_2$	$k = 2.0x10^{-12}$

Table 3.2. Continued - Reactions in DMS Model and respective rate constants

Reaction	Rate Constant, k[a]
32. $CH_3SO + HO_2 \rightarrow CH_3SO_2 + OH$	$k = 1.5x10^{-12}$
33. $CH_3SO + CH_3SO \rightarrow CH_3SO_2 + CH_3S$	$k = 7.5x10^{-12}$
34. $CH_3SO_3 + CH_2O \rightarrow CH_3SO_3H + CHO$	$k = 1.6x10^{-15}$
35. $CH_3S(O)(OH)CH_3 + O_2 \rightarrow CH_3S(O)CH_3 + HO_2$	$k = 1.2x10^{-12}$
36. $CH_3SOH + OH \rightarrow CH_3SO + H_2O$	$k = 1.1x10^{-10}$
37. $SO_2 + OH \rightarrow HOSO_2$	$k = 1.1x10^{-12}$
38. $HOSO_2 + O_2 \rightarrow SO_3 + HO_2$	$k = 4.0x10^{-13}$
39. $HOSO_2 + OH \rightarrow H_2SO_4$	$k = 1.0x10^{-11}$
40. $SO_3 + H_2O \rightarrow H_2SO_4$	$k = 9.1x10^{-13}$
41. $CH_3SO_3 + HO_2 \rightarrow CH_3SO_3H + O_2$	$k = 5.0x10^{-11}$
42. $CH_3SOH + CH_3SO_3 \rightarrow CH_3SO_3H + CH_3SO$	$k = 3.4x10^{-12}$
43. $CH_3SOOO \rightarrow CH_3SO + O_2$	$k = 1.7x10^{2}$
44. $CH_3SOOO + CH_3S \rightarrow CH_3SO + CH_3SO_2$	$k = 7.0x10^{-11}$
45. $CH_3SOOO + NO \rightarrow CH_3SO_2 + NO_2$	$k = 8.0x10^{-12}$
46. $CH_3SO_2 + O_2 \rightarrow CH_3S(O)_2OO$	$k = 2.6x10^{-18}$
47. $CH_3S(O)_2OO \rightarrow CH_3SO_2 + O_2$	$k = 3.3x10^{6}$
48. $CH_3S(O)_2OO + NO \rightarrow CH_3SO_3 + NO_2$	$k = 1.0x10^{-11}$
49. $CH_3S(O)_2OO + CH_3S \rightarrow CH_3SO_3 + CH_3SO$	$k = 6.0x10^{-11}$
50. $CH_3S + NO \rightarrow CH_3SNO$	$k = 2.87x10^{-11}$
51. $CH_3SNO \xrightarrow{h\nu} CH_3S + NO$	$k = 0.5k_{NO_2}$
52. $CH_3SSCH_3 \rightarrow Wall$	$k = 0.0$
53. $SO_2 \rightarrow Wall$	$k = 0.0$
54. $H_2O_2 \xrightarrow{h\nu} 2\ OH$	$k = 7.1x10^{-4}k_{NO_2}$
55. $CH_3SCH_2OO + CH_3S \rightarrow CH_3SCH_2O + CH_3SO$	$k = 6.1x10^{-11}$
56. $CH_3SCH_2OO + CH_3SO \rightarrow CH_3SCH_2O + CH_3SO_2$	$k = 4.0x10^{-12}$
57. $CH_3SCH_2OO + CH_3SO_2 \rightarrow CH_3SCH_2O + CH_3SO_3$	$k = 2.5x10^{-13}$
58. $CH_3SCH_2OO + CH_3SCH_2OO \rightarrow CH_3SCH_2O + O_2$	$k = 8.6x10^{-14}$
59. $CH_3SCH_3 + NH_3 \rightarrow CH_3S(NO_3)CH_3$	$k = 7.5x10^{-13}$
60. $CH_3S(NO_3)CH_3 \rightarrow CH_3SCH_2 + HONO_2$	$k = 1.2x10^{2}$
61. $CH_3SCH_3 + NO_2 \rightarrow CH_3S(O)CH_3 + NO$	$k = 9.0x10^{-21}$
62. $CH_3SCH_3 \rightarrow aerosol$	$k = 3.73x10^{-6}$*
63. $SO_2 \rightarrow Aerosol$	$k = 1.81x10^{-4}\ s^{-1}$*

*Rates that were optimized in this work. [a]Rate constants are in units of molecules, cm^3 and sec.

3.2.1 DMS Benchmarking

For the DMS kinetic model's benchmarking only one set of SIFT-MS data was available to benchmark against. This data was from chamber gas-phase experiment of DMS reacting with H_2O_2 with UV lamps on. The ion counts from the SIFT-MS are calibrated. Since it is calibrated, a 20% decrease on the SIFT ion count data means a 20% decrease in concentration, so this quantitative data allows for estimations of DMS, but cannot be used to compare relative amounts of different compounds. As shown in Figure 3.6 only the oxidation of DMS was used. In this figure the modeled concentration of DMS is represented by the solid black line and the SIFT-MS ion counts obtained from chamber experiments by the blue points. The modeled concentrations of DMS in Figure 3.6 are the concentrations obtained by the kinetic model only accounting for gas-phase reactions and not aerosol formation. For this reason, the concentration of DMS that is oxidized according to the kinetic model is much lower compared to what it is observed from the experimental data. Also, the rate of DMS loss is considerably slower than what is observed for DMDS, in fact, about 3.5 times slower the rate at which the concentration of DMS in Figure 3.1 decreases. The experimental data used to benchmark the kinetic model for DMS is the average of the data collected from the chamber experiment. The experimental data was collected in intervals of 5 min, so that the average concentration of each 5 min interval was used to benchmark the DMS kinetic model against. This was done because the intervals had scattered data points across the duration of each interval collected throughout the experiment due to instrumentation issues with the equipment used in the chamber experiments. Thus, the averages of this data were used to better represent the

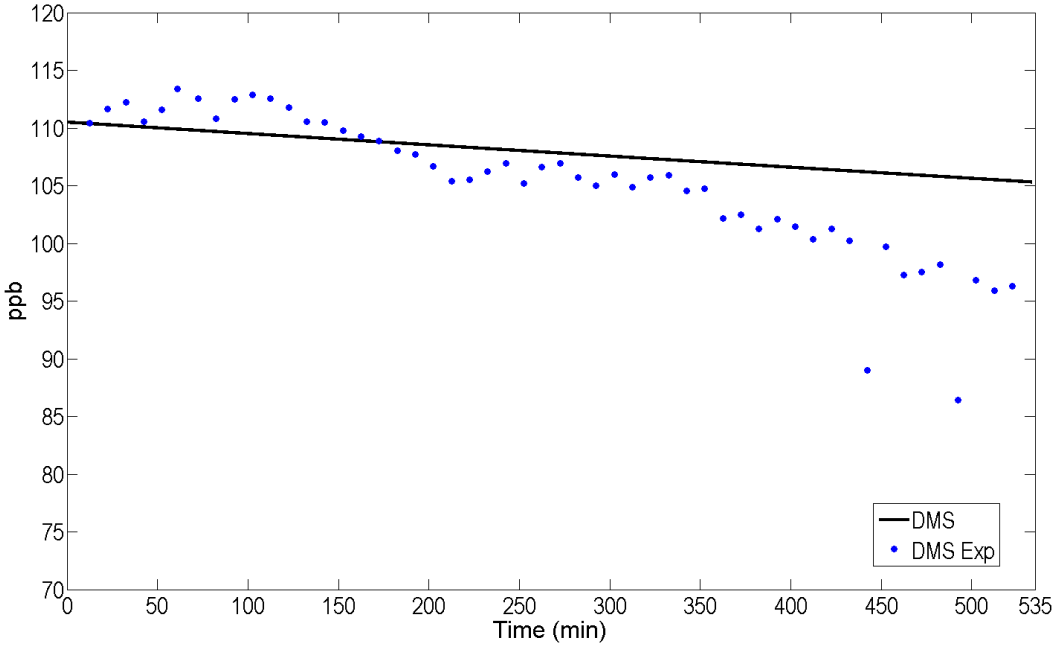

Figure 3.6 Comparison of modeled concentration and calibrated SIFT-MS ion counts as a function of time of DMS. No aerosol formation rates. Black solid line represents the concentration from the kinetic model while the blue markers show the SIFT-MS ion counts.

concentration of DMS in each of the data intervals. From Figure 3.6 a clear pattern of decreasing concentration of DMS is observed. In the experimental gas-phase data it decreases from its initial concentration of 110.5 to 97 ppb, which is a decrease of 11.82% from the initial concentration. Figure 3.6 also shows the model concentration of DMS decrease from 110.5 to 105 ppb, this difference in concentration from experimental to modeled DMS oxidation can be due to aerosol formation.

3.2.2 Gas-to-aerosol Optimized Rate for DMS

The initial proposed model in the first stage of the DMS kinetic model study showed a difference in DMS concentration. To proceed on making the model more accurately represent the gas-phase experimental data a rate of gas-to-aerosol formation for DMS was

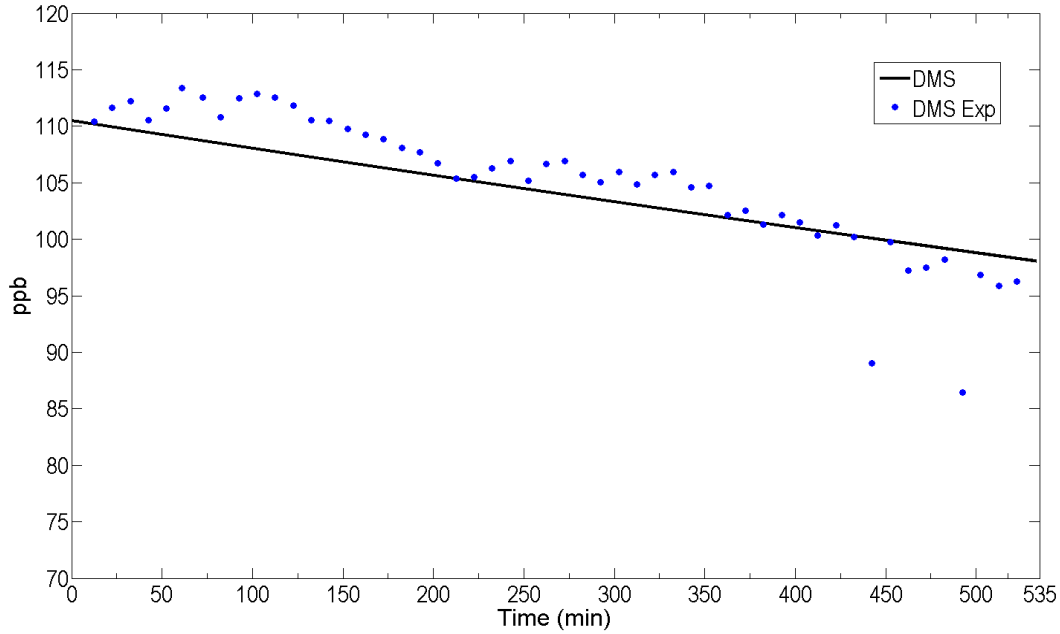

Figure 3.7. Comparison of DMS concentration as a function of time of modeled data and SIFT-MS ion counts with optimized of gas-to-aerosol rate. Aerosol formation rate for DMS was optimized, and the black solid line represent the data from the model while the blue markers show the SIFT-MS data.

included into the model. This gas-to-aerosol rate was then optimized to achieve the best possible fit to the DMS experimental concentrations while keeping the rest of the rates constant. This allowed the concentrations of the gas-phase DMS have a better fit to the experimentally observed concentrations, as observed in Figure 3.7.

The gas-to-aerosol rate optimized previously in the DMDS model for SO_2 was also included in this model. The optimized value for the DMS gas-to-aerosol rate is 3.73×10^{-6} s^{-1} for DMS and gave the lowest possible least squares value (**S**) of 1173.03. This optimized gas-to-aerosol is pseudo-first order and was incorporated to better estimate the amounts of sulfur that would be expected to be found in the aerosol particles and to reduce the error from sulfur content estimations in aerosols. In Figure 3.7, the oxidation of DMS from the kinetic model is in closer agreement with the experimental concentations, as the modeled

DMS concentration decreases from 110 ppb to around 97 ppb. Thus, the implementation of the gas-to-aerosol rate gives a more accurate simulation of the aerosol formation chamber experiments. After benchmarking the DMS concentrations of the kinetic model against the experimental data, the next step was to look at the formation of SO_2, DMSO, and other by-products from the oxidation of DMS.

3.2.3 Modeled Concentrations of SO_2, DMSO, MSA, and CH_3SOH

Although no experimental data from the atmospheric chamber was available for other compounds apart from DMS, the next step on the study was to look at their concentrations according to the kinetic model to seek insight on qualitative undestanding of the atmospheric oxidation process of DMS. Apart from the formation of SO_2 and MSA, one of the most important features that were relevant on this DMS model was the formation of DMSO, which branches off from the formation of $CH_3S(OH)CH_3$ from the OH-addition pathway shown in Scheme 2.2. The formation of DMSO in this mechanism would readily

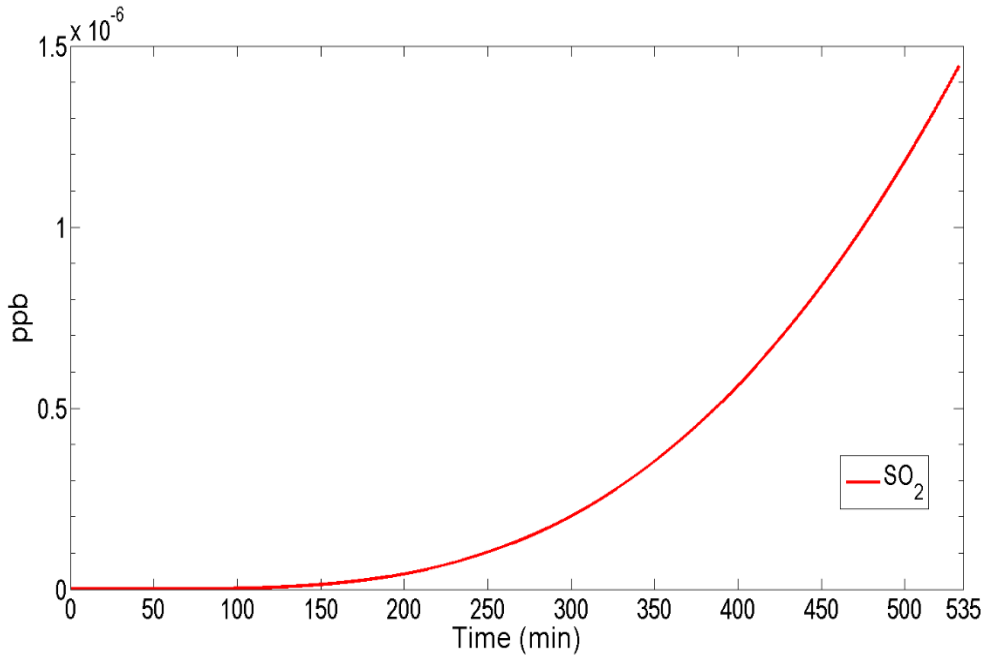

Figure 3.8. Concentration as a function of time from DMS atmospheric oxidation model of SO_2.

diminish the amount of SO_2, as the chemical stability of DMSO would prevent the further oxidation of the reduced sulfur species into SO_2. Because of this, comparing the amounts of DMSO and SO_2 being formed according to the kinetic model would help deteming which initial oxidative pathway is favored in the mechanism. Figure 3.8 shows the change in concentration over time of SO_2 according to the DMS kinetic model, where SO_2 concentration increases from 0 to 1.44×10^{-6} ppb.

Then, Figure 3.9 shows the concentration of the DMSO, its concentration increases from 0 to 6.9×10^{-5} ppb. These seem to be much lower than that of the concentrations observed in atmospheric chamber experiments as concentrations in the range of 6-10 ppb of SO_2 have been observed. Compared to SO_2, the formation of DMSO is favored, with concentrations of one order of magnitud higher. Because SO_2 is of great enviromental concern due to being a known precursor of sulfate aerosols. The favored formation of

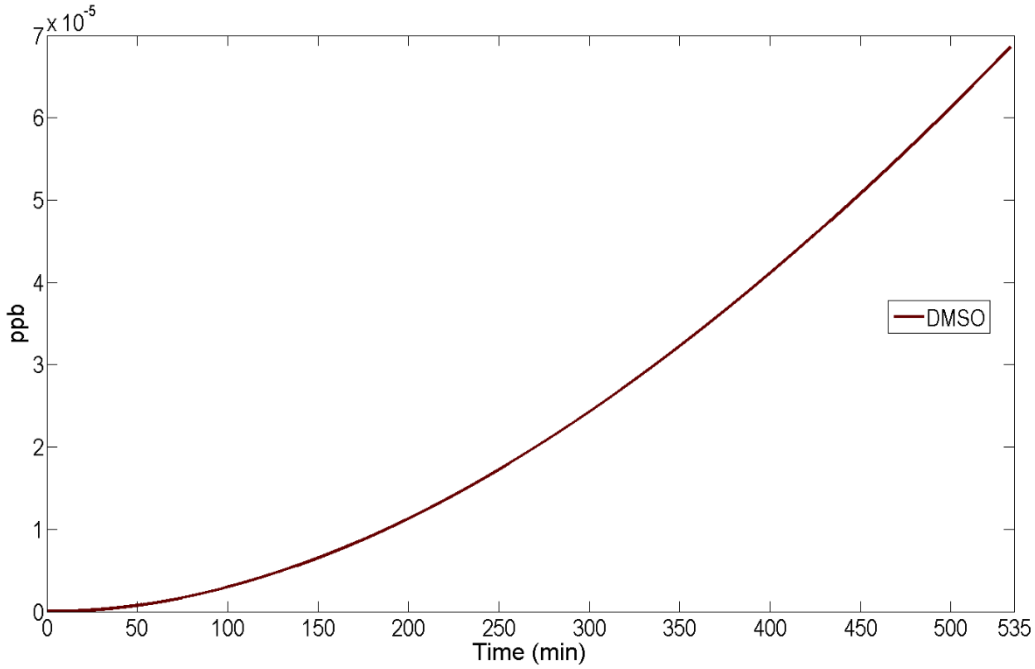

Figure 3.9. Concentration as a function of time from DMS atmospheric oxidation model of DMSO.

DMSO from the atmospheric oxidation of DMS might be of consideration towards the study and development of particle formation mechanisms.

Other organosulfur compouds worth studying from this kinetic model of DMS include MSA and CH_3SOH. MSA has been observed by other research groups during laboratory experiments. They contribute towards the formation of aerosol particles in the presence of water and low-volatility amine mixtures. Aerosol nucleation is enhanced under these conditions.[48] Figure 3.10 shows the modeled concentrations of MSA from the kinetic model of the atmospheric oxidation of DMS. The modeled highest concentration of MSA from the oxidation of 110.5 ppb of DMS is merely 1.28×10^{-36} ppb, which would be much lower than the detection limits of the chamber facility instrumentation. MSA might not be even detected in the chamber experiments if concentrations this low are persistent throughout these experiments. The GC from the chamber can detect DMSO, but it has

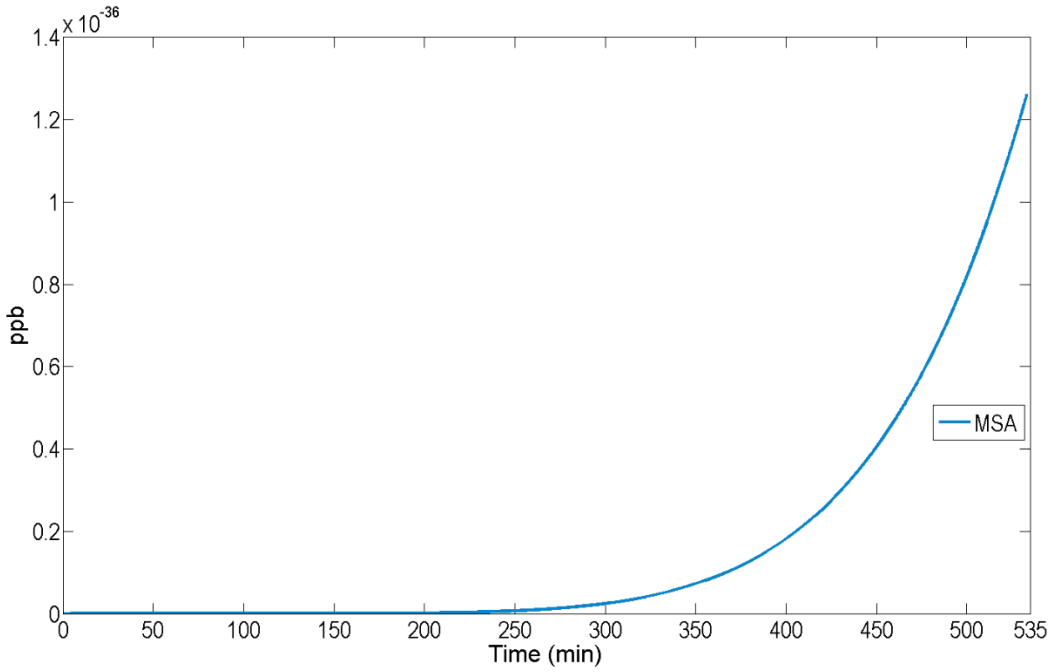

Figure 3.10. Concentration as a function of time of MSA from DMS atmospheric oxidation kinetic model.

never been formed in any of the smog chamber experiments from collaborators to date. However, DMSO has been seen in ambient experiments, especially in the presence of fog, which might suggest the aqueous pathways to be relevant on the formation of DMSO.

In contrast with the low concentrations of MSA and SO_2 predicted by the DMS kinetic model, the modeled concentrations of CH_3SOH are significantly higher than the other species presented here in this work for this specific model. Figure 3.11 shows the increasing concentration of CH_3SOH from the DMS model, this compound is formed in the highest concentrations from this model. This supports the theory that the OH-addition pathway is favored. The CH_3SOH concentration increases from 0 to 6.8×10^{-3} ppb throughout the 530-min duration of the experiment. This concentration is around 2 orders of magnitude higher than that of DMSO, which is the compound with the second highest concentration from the DMS model.

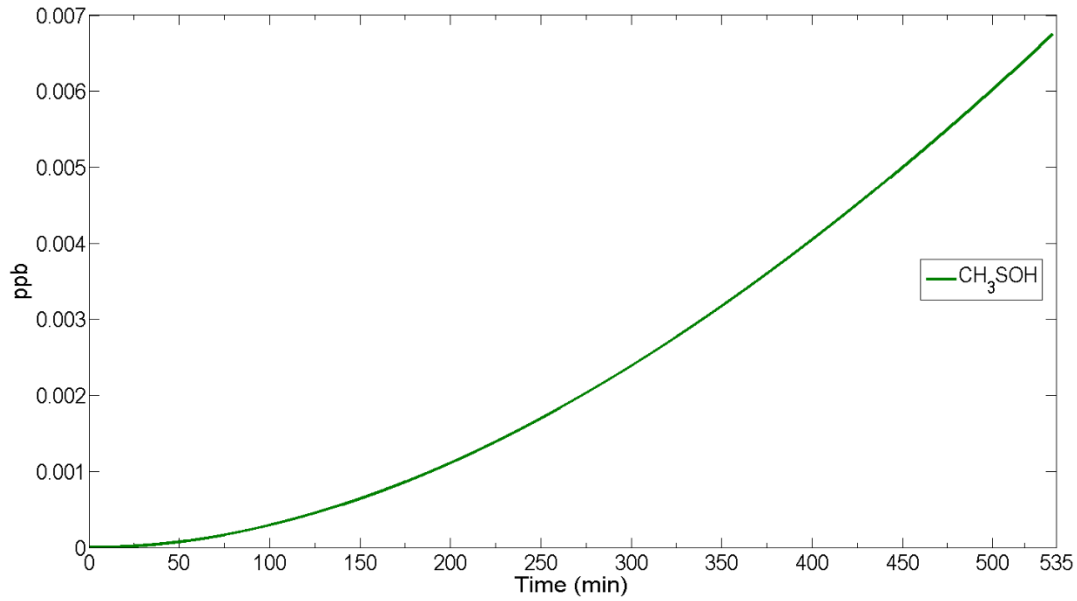

Figure 3.11. Concentration as a function of time from DMS atmospheric oxidation model of CH_3SOH.

As seen in Figure 3.7 the DMS kinetic model as well as the chamber experimental concentrations, shows a loss ~13 ppb of the parent compounds DMS. However, the concentrations of sulfur containing products estimated by the kinetic model of the gas-phase oxidation of DMS only account for ~0.007 ppb in total. Representing a great discrepancy in concentrations from the amount of lost DMS and product formations. This could be attributed to aerosol formation from one or several compounds from the kinetic model. Determining which compound(s) must be priority for future research.

3.3 TMA Kinetic Model

Sulfur- and nitrogen-containing compounds are both known to be produced from agricultural, industrial and natural sources, and interactions between S and N have shown to enhance the formation of aerosols. Thus, low-volatility amines are also of interest from the aerosol particle formation perspective. [32,34,46,59] After the kinetic modeling of DMDS and DMS which are two of the most atmospherically relevant reduced sulfur species, the study and development of kinetic models for relevant atmospheric nitrogen containing compounds became the next step of this research. This led to the development of a kinetic model for trimethylamine (TMA), a low-volatility amine compound which has been observed in atmospheric aerosol studies. The reactions included in the TMA model are shown in Table 3.3, where the rate constants for some of these reactions had to be optimized due to lack of previous publications on the literature about the rate constants for reactions. The model includes a total of 15 reactions, however, the reactions for the dissociation of N_2O_5 and formation of NO_x species were also included in the model but are not explicitly included in Table 3.3. [43] From this model the rate constants for Reactions 1, 3, 4, 5, 10, 16, 17, 18, 19 and 20 were optimized in order to find the values that best represented the

experimental data that was used to benchmark the gas-phase oxidation mechanism against. From this mechanism there are three oxidative pathways that affect TMA, the first one is photooxidative cleavage of one of the methyl groups shown in Reaction 10. The second pathway is H- abstraction, which occurs in two ways, either photolytic H- abstraction, shown in Reaction 1, or H-atom abstraction via an OH radical, shown in Reaction 2.

Table 3.3. Reactions included in TMA Model with their respective rate constants. Adapted from Ref 43. [49]

Reaction	Rate Constant, k[a]
1. $(CH_3)_3N \xrightarrow{h\nu} (CH_3)_2NCH_2$	$k = 4.30x10^{-3}$*
2. $(CH_3)_3N + OH \rightarrow (CH_3)_2NCH_2 + H_2O$	$k = 6.11x10^{-11}$
3. $(CH_3)_2NCH_2 \xrightleftarrows{O_2/NO} (CH_3)_2NCH_2O$	$k = 1.0x10^{-1}$ *
4. $(CH_3)_2NCH_2O + O_2 \rightarrow (CH_3)_2NCHO + HO_2$	$k = 8.0x10^{-18}$*
5. $(CH_3)_2NCH_2O \rightarrow (CH_3)_2N + HCHO$	$k = 7.0x10^{-5}$*
6. $(CH_3)_2N + NO_2 \rightarrow (CH_3)_2NNO_2$	$k = 3.17x10^{-13}$
7. $(CH_3)_2N + O_2 + NO_2 \rightarrow CH_3NCH_2$	$k = 1.48x10^{-6}$
8. $(CH_3)_2N + NO \rightarrow (CH_3)_2NNO$	$k = 8.54x10^{-14}$
9. $(CH_3)_2NNO \xrightarrow{h\nu} (CH_3)_2N + NO$	$k = 1.0x10^{-3}$
10. $(CH_3)_3N \xrightarrow{h\nu} (CH_3)_2N + CH_3$	$k = 1.0x10^{-6}$ *
11. $CH_3 + NO_2 \rightarrow CH_3ONO$	$k = 1.26x10^{-3}$
12. $(CH_3)_2N + NO_2 \rightarrow CH_3NCH_2$	$k = 22.0$
13. $CH_3 + OH \rightarrow HCHO + H_2$	$k = 4.17x10^{-5}$
14. $CH_3 + NO_2 \rightarrow HCHO + HNO$	$k = 46.50$
15. $CH_3 + O_2 \rightarrow HCHO + OH$	$k = 1.01x10^{-14}$
16. $(CH_3)_2NCHO \xrightarrow{OH} 0.35CH_3N(CHO)_2 + 0.65(CH_3)_2N$	$k = 14.4x10^{-8}$*
17. $CH_3NCH_2 \rightarrow aerosol$	$k = 1.0x10^{-4}$*
18. $HCHO \rightarrow aerosol$	$k = 4.0x10^{-5}$*
19. $(CH_3)_2NCHO \rightarrow aerosol$	$k = 1.7x10^{-5}$*
20. $CH_3N(CHO)_2 \rightarrow aerosol$	$k = 8.5x10^{-5}$*

*Rates that were optimized in this work. [a]Rate constants are in units of molecules, cm^3 and sec.

Then, a branching occurs after the formation of $(CH_3)_2NCH_2O$, as shown in Reaction 4 and 5, this compound leads to the formation of $(CH_3)_2NCHO$ and $(CH_3)_2N$ radical. From $(CH_3)_2N$ there is a branching to produce CH_3NCH_2, $(CH_3)_2NNO$, and $(CH_3)_2NNO_2$, which are shown in Reactions 6, 7, 8, 9, and 12. To reduce the number of parameters that needed optimization, three reactions corresponding to three of these rate constants that needed to be optimized were simplified into Reaction 3. Because of this, Reaction 3 represents the sum of an equilibrium and a forward reaction steps that incorporates three rate constants that needed to be optimized into one rate constant value for simplicity purposes. Table 3.4 shows the three different reactions that Reaction 3 from Table 3.3 encapsulates.

Table 3.4 Reactions Incorporated into reaction 3 from Table 3.3.

1. $(CH_3)_2NCH_2 + O_2 \rightarrow (CH_3)_2NCH_2OO$
2. $(CH_3)_2NCH_2OO \rightarrow (CH_3)_2NCH_2 + O_2$
3. $(CH_3)_2NCH_2OO + NO \rightarrow (CH_3)_2NCH_2O + NO_2$

3.3.1 TMA Benchmarking

The experimental data from TMA reacting with H_2O_2 with UV lamps on and only background NO_x from chamber experiment used to benchmark the TMA kinetic model is presented in Figure 3.12. This data includes six sets ion counts data from the SIFT-MS corresponding to the parent compound, in this case TMA, and the gas-phase products formed during the experiment. The ion counts are not calibrated, so this SIFT data only allows for estimations of individual compounds patterns. Thus, an increase on one of the peaks does indicate an increase on the concentration of that assigned compound, but it does not allow for relative amounts of different compounds to be known. From the products,

one of the sets of data had an unknown chemical composition, which seemed to match closely to the concentration of N-formyl-N-methylformamide after benchmarking of the kinetic model. However, the experimental data included ion counts data of N-dimethylformamide, N-methylmethanimine, formaldehyde, and nitromethane, the chemical structures of these compounds are presented in Chart 3.1

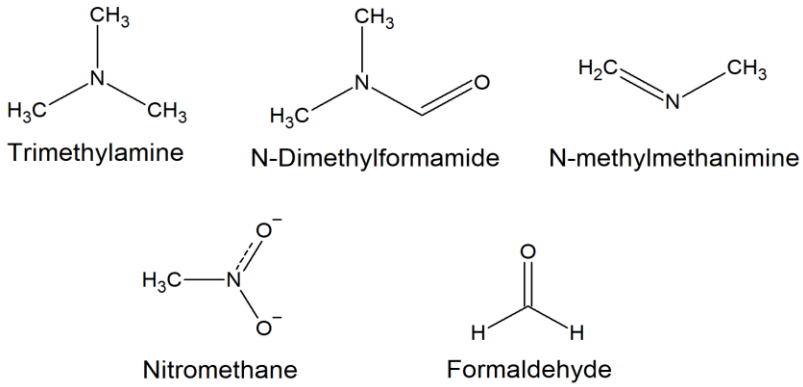

Chart 3.1 Chemical structures of compounds included in the experimental data used to benchmark the TMA kinetic model.

As seen in Figure 3.12, the photooxidation of TMA leads to the formation of several nitrogen containing compounds as well as formaldehyde and decrease in the initial concentration of TMA from 53.56 to 7.50 counts is observed. The product formed in most abundance is dimethylformamide, with a final of 10 counts. Then formaldehyde and methylmethanimine are second and third on abundance, with final concentrations of 7.5 and 5.5 counts respectively. At last, the compound with lowest concentration product being nitromethane, with 4.9 counts, followed by the unknown compound.

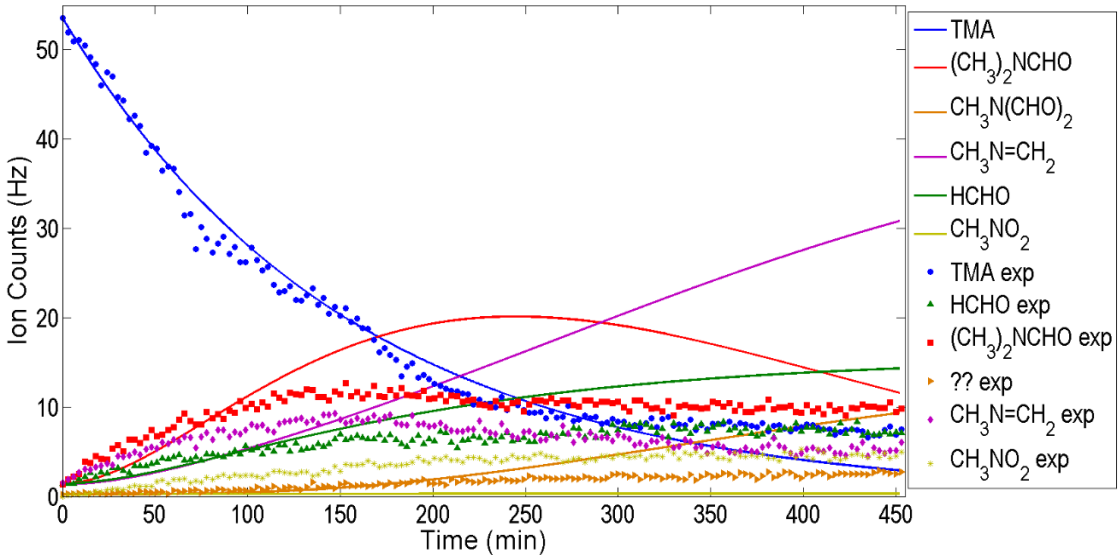

Figure 3.12 Ion counts from SIFT-MS as a function of time of TMA, HCHO, $(CH_3)_2NCHO$, $CH_3N=CH_2$, CH_3NO_2 and unknown species compared to modeled kinetic data.

3.3.2 TMA Oxidation Rates

Due to the large number of rate constant values that needed to be optimized from the TMA kinetic model presented in Table 3.3, the optimization of the reaction rates for the oxidation of TMA were optimized first. This was done by giving arbitrary initial rate constant values to Reactions 1, and 10, which are the reactions affecting the oxidation of the parent compound TMA. Then those values were optimized until the lowest least squares value for the compared TMA experimental and kinetic model concentrations was obtained. Figure 3.13 shows the compared TMA concentrations from the kinetic model and the ion counts from chamber experiments. As seen from Figure 3.12, the model has a great agreement of the experimental data from 0 min until 320 min, at which point the experimental ion counts of TMA plateau around 8 ppb until the end of the experiment while the TMA concentration from the kinetic model continues to decrease until it reaches end of the experiment with 4 counts. The lowest least squares value (**S**) obtained for TMA

concentration was 7.4903×10^{6} after the optimization of the rate constants of Reactions 1, 2, and 10. Consecutively, the rate constants of Reactions 3, 4, 5, and 9 were optimized in order to achieve the best possible fit to the experimental concentration. of the products expected to be generated from the oxidation of TMA, as shown in Figure 3.12.

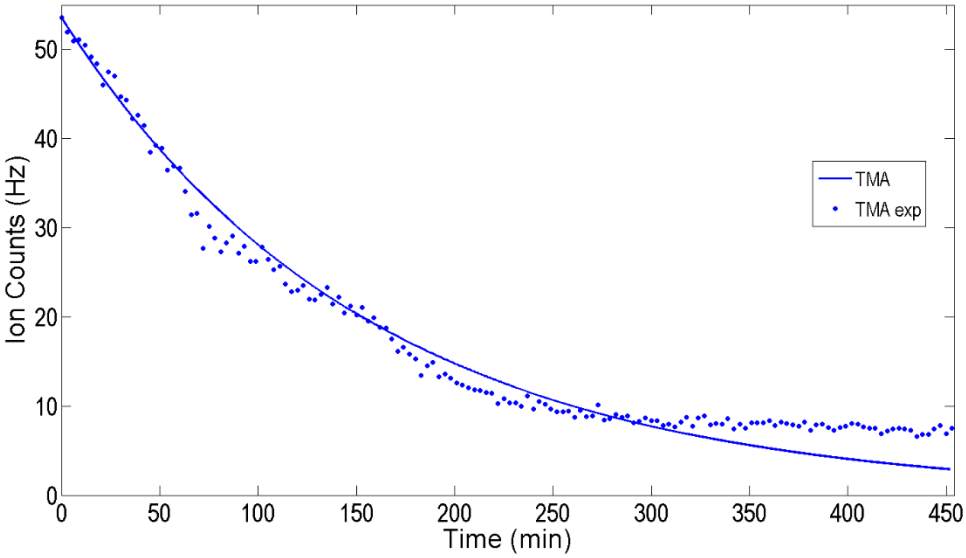

Figure 3.13 Ion counts from SIFT-MS as a function of time of the TMA compared to concentrations from the TMA kinetic model. Oxidation rates for TMA were optimized. Blue solid line represents the data from the model while the blue markers show the experimental data.

3.3.3 Products Rate Optimization

After optimizing the rate constants of the oxidation reactions of TMA, the rates of formation of the products were the next step on the optimization of the kinetic model. For this part of the study experimental data from the chamber experiments was available for four of the expected products to form from the gas-phase oxidation of TMA, which are shown in Chart 3.1. The optimization of the rate constants of reactions 3, 4, 5, 10, and 16 was necessary, and was done using the least squares methods as well. The optimized values for these rates are shown in Table 3.3. The modeled concentrations from the TMA kinetic

model and the experimental ion counts from the chamber experiments of the products is compared in Figure 3.14, where the solid colored lines represent the concentrations obtained from the kinetic model and the markers represent the experimental ion counts. As can be seen from Figure 3.14, the kinetic model achieves good agreement with only the first 100 min of the experimental data being benchmarked except for the compounds $CH_3N{=}CH_2$ and CH_3NO_2. As the model was first optimized to fit the initial rapid formation rates of the products, however, fails to replicate the decrease in counts that experimental data show for HCHO, $(CH_3)_2NCHO$, and $CH_3N(CHO)_2$ during the final 250 min of the experiment.

In the case of CH_3NO_2, the concentration estimated by the kinetic model shows to be much lower compared to the experimentally observed ion counts, and almost non-increasing. For $(CH_3)_2NCHO$ the kinetic model estimates an excess of ~2 counts from the

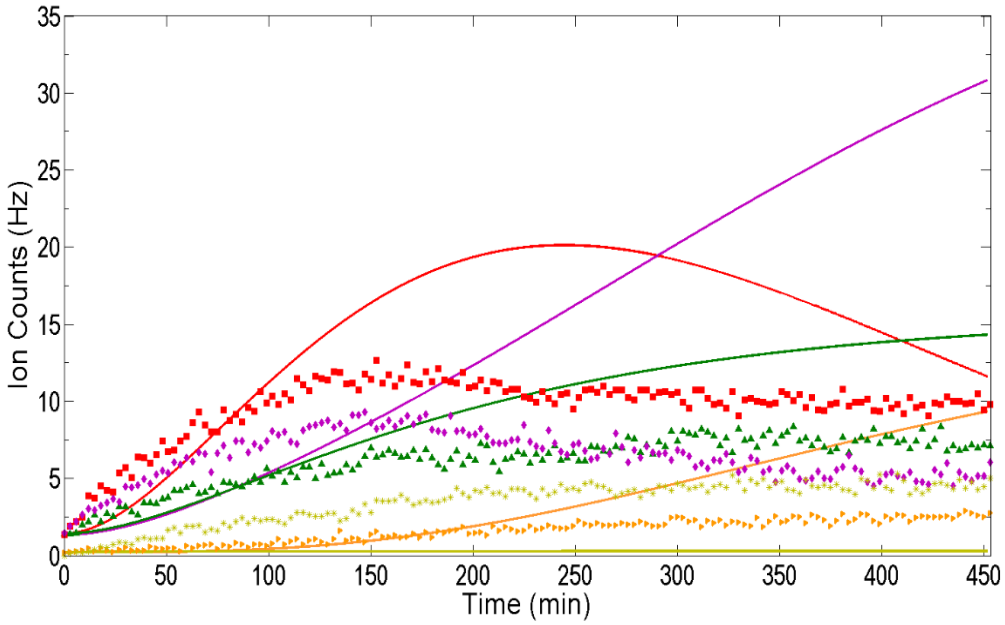

Figure 3.14 Ion counts from SIFT-MS as a function of time of the oxidation products compared to concentrations from the TMA kinetic model. Compounds HCHO, $(CH_3)_2NCHO$, $CH_3N{=}CH_2$, CH_3NO_2 and $CH3N(CHO)_2$. No Gas-to-aerosol rates included.

observed experimental final concentration, but it fails to simulate the plateau concentrations observed from the 200-min mark and onwards. For the compounds HCHO, $(CH_3)_2NCHO$, and $CH_3N(CHO)_2$ a similar trend is observed, as the initial rates of formation of the products, up to the 100-min mark, present good agreement to the experimental data, however the late decrease and plateau of the concentrations of these products is not achieved by the kinetic model. The kinetic model shows an excess in the final concentrations of HCHO, $CH_3N{=}CH_2$, and $CH_3N(CHO)_2$, which corresponds of 7 counts for HCHO, 25 counts for $CH_3N{=}CH_2$, and 7 counts for $CH_3N(CHO)_2$.

As discussed with the previous model, this excess in concentration that the kinetic model estimates, could be attributed to the absence of aerosol formation rates, the absence of other oxidation or reverse reactions that have not been considered, or wall adsorption of the nitrogen compounds. Thus, to obtain better agreement with the experimental data, especially on the last 300 minutes of the experiment, rates of compound loss or gas-to-aerosol rates were included and optimized to the kinetic model. Four of these gas-to-aerosol rates were incorporated, one for each of the compounds $(CH_3)_2NCHO$, HCHO, $CH_3N{=}CH_2$, and $CH_3N(CHO)_2$. The values of the optimized gas-to-aerosol ratios are presented in Table 3.3 reactions 16 – 20. Figure 3.15 shows the concentrations of the products from the oxidation of TMA from the kinetic model with the optimized gas-to-aerosol rates compared to the experimental concentrations from the chamber experiments.

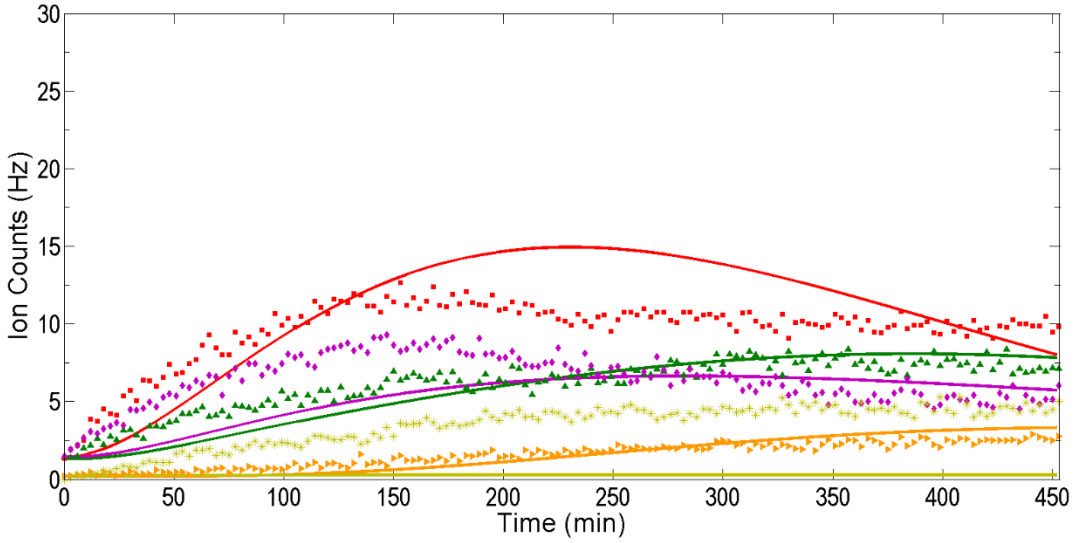

Figure 3.15 Ion counts from SIFT-MS as a function of time of the oxidation products compared to concentrations from the TMA kinetic model. Compounds HCHO, $(CH_3)_2NCHO$, $CH_3N(CHO)_2$, $CH_3N{=}CH_2$, CH_3NO_2. Gas-to-aerosol rates are included.

As shown in Figure 3.15, the optimized gas-to-aerosol loss rates give the model a closer fit to the experimental concentrations of the products and give lower least squares values (**S**) for each compound being benchmarked. The least squares values (**S**) after the optimization of the rate constants for each of the compounds being benchmarked from this model are 1.6169×10^{6} for HCHO, 1.0377×10^{7} for $(CH_3)_2NCHO$, 1.8072×10^{7} for CH_3NO_2, and 1.1394×10^{7} for $CH_3N{=}CH_2$. The modeled concentration of CH_3NO_2 remains much lower than the experimental data for this compound, even after the optimization of the rate constants. However, the modeled concentrations of HCHO, $(CH_3)_2NCHO$, and $CH_3N(CHO)_2$ show a much better agreement to the experimental data. Even while this is true, the $CH_3N{=}CH_2$ concentration does not accurately represent the experimental data until after 250-min mark of the experiment.

4 Summary and Conclusions

The goals of this project were (1) to compare and optimize the previously reported kinetic mechanisms for the gas-phase atmospheric oxidation mechanisms of DMDS and DMS; (2) to optimizing reaction rates and (3) to develope a kinetic model of the gas-phase photooxidation mechanism of TMA to gain insight into the process of aerosol particle formation from the gas-phase oxidation of these compounds. This lays fundation for developing kinetic models for the heterogenous mixtures of atmospherically relevant sulfur and nitrogen containing compounds.

4.1 Incorporation of Gas-to-Aerosol Rates

Comparing the mechanisms of DMDS and DMS to experimental concentrations from atmospheric chamber experiments without adding and optimizing gas-to-aerosol reactions showed a consistent overestimation on the concentrations obtained from the kinetic models for DMDS and SO_2 from the DMDS kinetic model and for DMS from the DMS kinetic model. This led to the inclusion of gas-to-aerosol pseudo first order reactions to procure the most accurate reproduction of the atmospheric chamber experimental data. The incorporation of gas-to-aerosol reactions into kinetic models for the gas-phase photooxidation of DMDS and DMS allowed for the optimzation of rate contants that represent the formation of SOA particles. The optimized gas-to-aerosol rate values for the DMDS and SO_2 that were incorporated into the DMDS kinetic model, which have the values of 0.58×10^{-4} s^{-1} for DMDS and 1.81×10^{-4} s^{-1} for SO_2, were able to bring the model to have better agreement with the experimental data to which it was benchmark against as shown in Figure 3.3. A similar approach was used to obtain a better agreement with the DMS kinetic model where a gas-to-aerosol was incorporated into the kinetic model and

optimized to a value of 3.73×10^{-6} s^{-1}. These gas-to-aerosol rates can be crucial in future work when comparing the effects of other compounds in the gas mixtures of chamber experiments, by giving a reference as to how much sulfur would be expected to be present in the aerosol particles when the only analyte in the chamber in DMDS or DMS compared to when two or more analytes are present in the gas mixture.

4.2 Differences in oxidative pathways between DMDS and DMS

As the outcome of the development and optimization of each kinetic model was studied, some observations regarding the mechanisms and by-products of each model were made. One of these obsevations was the fundamental differences on the chemical structures of DMDS and DMS leading to very different outcomes in terms of products forming in different concentrations and favoring different oxidative pathways. The difference in oxidative pathways affect the two reduced-sulfur compounds DMDS and DMS in their rate of atmospheric oxidation due to DMDS favoring the photolitic oxidation poathway. As can be seen from the kinetic models in Tables 3.1 and 3.2, the photooxidative pathway described in reaction 21 from Table 3.1 plays a relevant role in the oxidation of DMDS that leads to the splitting of the parent compound into two $CH_3S^{\cdot}$ molecules, while the same is not applicable to DMS. This charachteristic photooxidative pathway is most favored due to the S-S bond of DMDS (CH_3SSCH_3) as data from this kinetic model suggests, from the rapid cleavage of the S-S bond from DMDS. This can be observed in Figure 3.5, where the formation of the radical species CH_3S and CH_3SO in high concentrations that are near the concentration of SO_2 is indicative of the hypothesis that the S-S bond dissociation is favored over the OH-addition pathway under these experimental conditions. It is worth noting that higher concentrations of OH in the

experimental conditions may act in favor of OH-addition, however, the rate constant for the photooxidation pathway is seven orders of magnitude larger than that of the OH-addition pathway, thus the fovorability of photooxidation might not be overcome simply by an increase on OH concentration.

The favorable formation of DMSO over SO_2 from the kinetic modeling of the oxidation mechanism of DMS (CH_3SCH_3), it can be attributable to the absence of a S-S bond. Since the photolytic dissociation of the S-C bond, which would be the mechanism that the dissociation of DMS would have to follow to generate $CH_3S^{\cdot}$ in a way similar to DMDS, is not energetically favorable, then the addition of OH is then the most favorable oxidative pathway for DMS. Thus, as Scheme 2.2 shows, the formation of $CH_3S(OH)CH_3$ followed by the branching from this compound into CH_3SOH or DMSO becomes they key step limiting the further oxidation of the sulfur compounds into SO_2. This can be seen from reactions 3 and 4 from Table 3.3, where the branching ratio of the intermediate compound $CH_3S(OH)CH_3$ is determined in favor to DMSO formation due to the inherently high concentrations of O_2 in the air.

4.3 Formation of MSA and CH_3SNO

One of the initial interests of this project was to evaluate if the formation of CH_3SNO could act as a kinetic trap that could prevent or at least to diminish the amount of SO_2 that was to be produced from the oxidation of either DMDS or DMS. For this reason, the reactions of formation and dissociation of CH_3SNO were incorporated into the kinetic models. The results shown from the kinetic models for DMDS and DMS after they were optimized estimated concentrations of 8.0×10^{-10} ppb and 6.0×10^{-20} ppb respectively of CH_3SNO. The low concentrations of this compound estimated by the models, the high

concentrations of SO_2 and DMSO formed from the kinetic model, and the rapid rate of photodissociation of the compound CH_3SNO itself invalidated the hypothesis that CH_3SNO could be a kinetic trap for the gaseous sulfur produced from the oxidation of DMDS and DMS.

Another interesting observation noticed from the kinetic models of DMDS and DMS is the low concentrations at which MSA was estimated to be formed from the oxidation of those compounds. The amount of MSA from experimental chamber experiments as well as other studies done my multiple research groups were found to be significantly higher compared to what the kinetic modeling predicts from the DMDS and DMS gas-phase oxidation models. For example, observations from field studies for example, have found that typical levels of atmospheric MSA are typically in the range of $\sim 10^5$-10^7 molecules cm^{-3}, which translates to a range of ~10% - 100% of that of typical atmospheric sulfate concentrations. In comparison, the kinetic model for DMDS predicted only a 3.6×10^{-11} % of that of the SO_2 concentration from chamber experiments, and the kinetic model for DMS shows an even more negligible amount of MSA is predicted. The discrepancy between the concentrations of the models and observed experimentally observed concentrations of atmospheric MSA might be further explained in furutre research when gas-phase experimental data from atmospheric chamber experiments of MSA concentration is available to compare with those predicted by the DMDS and DMS kinetic models and benchmark against. Conversely, if no detection of MSA is obtained in future atmospheric chamber experiments, it might be an indication that the amount of MSA being produced from the oxidation of DMDS and DMS in the experimental concentrations used in this

study are under the lower limits of detection of the instrumentation used in the chamber facility as suggested by the kinetic models.

4.4 TMA Products Fitting

The fitting of the products from the oxidation of TMA was challenging due to the number of rate constants that required to be optimized. As seen from Figure 3.15, the optimization of the kinetic model of gas-phase oxidation of TMA generated good agreement with only the initial 100 min of the experimental concentrations against which it was being benchmarked for all the products with exception of the compound CH_3NO_2. Although better agreement in the final stage of the experiment was achieved by the incorporation of optimized gas-to-aerosol rates, this kinetic model fails to replicate the rapid increase in concentration that experimental data for $CH_3N{=}CH_2$ show during the initial 225 min of the experiment. In the case of CH_3NO_2 the concentration estimated by the kinetic model is much lower than the experimentally observed concentrations. The incorporation of other reactions that provide a faster formation of the products $CH_3N{=}CH_2$ and CH_3NO_2 is a plausible direction for future work towards betterment of this kinetic model and obtaining a more accurate simulation of the experimental concentrations as observed from the chamber experiment. Another approach to the discrepancy in the products concentrations might be studying and quantifying the effects that the Teflon® walls of the chamber have on each of the products as well as the parent compound, since reported adsorption onto the walls has been reported in past experiments for amine compounds. Chamber experiments and kinetic modeling of these gas-to-wall effects would likely lead to better reproducibility of chamber experiments data from the kinetic model. This will lead to optimization of rate constants for the formation of aerosol particles from

TMA gas-phase oxidation as well as more accurate optimization of rate constants of the reactions already included in this model. Doing so will help develop kinetic models for other atmospherically relevant amine and nitrogen containing species, such as DEA and NH_3. This will also help in the study of atmospheric oxidation of mixtures of amine and sulfur containing compounds, which will lead to better understanding of the complex mechanisms of SOA formation from gas-phase compounds that are prominent in some farm and animal waste.

BIBLIOGRAPHY

(1) Boucher, O. In *Atmospheric Aerosols: Properties and Climate Impacts*; Springer, 2015; pp. 9–160.

(2) Grassian, V. H.; Stone, E. A. Chemistry's Contributions to Our Understanding of Atmospheric Science and Climate. *J. Chem. Educ.* **2015**, *92* (4), 595–597.

(3) Perraud, V.; Horne, J. R.; Martinez, A. S.; Kalinowski, J.; Meinardi, S.; Dawson, M. L.; Wingen, L. M.; Dabdub, D.; Blake, D. R.; Gerber, R. B.; et al. The Future of Airborne Sulfur-Containing Particles in the Absence of Fossil Fuel Sulfur Dioxide Emissions. *Proc. Natl. Acad. Sci. USA.* **2015**, *12* (44), 13514–13519.

(4) Ghan, S. J.; Schwartz, S. E. Aerosol Properties and Processes: A Path from Field and Laboratory Measurements to Global Climate Models. *Bull. Am. Meteorol. Soc.* **2007**, *88* (7), 1059–1084.

(5) *Climate Change 2014: Synthesis Report*; IPCC: Geneva, Switzerland, 2015.

(6) Manzoor, S.; Kulshrestha, U. Atmospheric Aerosols: Air Quality and Climate Change Perspectives. *Curr. World Environ.* **2015**, *10* (3), 738–746.

(7) Faloona, I.; Conley, S. A.; Blomquist, B.; Clarke, A. D.; Kapustin, V.; Howell, S.; Lenschow, D. H.; Bandy, A. R. Sulfur Dioxide in the Tropical Marine Boundary Layer: Dry Deposition and Heterogeneous Oxidation Observed during the Pacific Atmospheric Sulfur Experiment. *J. Atmos. Chem.* **2009**, *63* (1), 13–32.

(8) Textor, C.; Schulz, M.; Guibert, S.; Kinne, S.; Balkanski, Y.; Bauer, S.; Berntsen, T.; Berglen, T.; Boucher, O.; Chin, M.; et al. Analysis and Quantification of the Diversities of Aerosol Life Cycles within AeroCom. *Atmos. Chem. Phys.* **2006**, *6* (7), 1777–1813.

(9) Wild, M.; Ohmura, A.; Makowski, K. Impact of Global Dimming and Brightening on Global Warming. *Geophys. Res. Lett.* **2007**, *34* (4), L04702.

(10) Mian, C.; Schwartz, S. E.; Kahn, R. A. *Atmospheric Aerosol Properties and Climate Impacts*; NASA: Washington, D.C, 2009.

(11) *Contribution of Working Groups I, II and III to the Fourth Assessment*; Climate Change 2007; Synthesis Report; IPCC: Geneva, 2008.

(12) Zhang, Y.; Rossow, W. B.; Stackhouse, P. W. Comparison of Different Global Information Sources Used in Surface Radiative Flux Calculation: Radiative Properties of the near-Surface Atmosphere. *J. Geophys. Res.* **2006**, *111* (D13), D13106.

(13) Haywood, J.; Boucher, O. Estimates of the Direct and Indirect Radiative Forcing due to Tropospheric Aerosols: A Review. *Rev. Geophys.* **2000**, *38* (4), 513–543.

(14) Twomey, S. The Influence of Pollution on the Shortwave Albedo of Clouds. *J. Atmos. Sci.* **1977**, *34* (7), 1149–1152.

(15) Albertch, B. A. Aerosols, Cloud Microphysics, and Fractional Cloudiness. *J. Microsc.* **1989**, *152* (3), 789–794.

(16) Liu, Y.; Daum, P. H.; McGraw, R. An Analytical Expression for Predicting the Critical Radius in the Autoconversion Parameterization. *Geophys. Res. Lett.* **2004**, *31* (6), L06121.

(17) Godleski, J. J.; Verrier, R. L.; Koutrakis, P.; Catalano, P.; Coull, B.; Reinisch, U.; Lovett, E. G.; Lawrence, J.; Murthy, G. G.; Wolfson, J. M.; et al. Mechanisms of Morbidity and Mortality from Exposure to Ambient Air Particles. *Res. Rep. Health Eff. Inst.* **2000**, *91*, 5-88; discussion 89-103.

(18) Bräuner, E. V.; Forchhammer, L.; Møller, P.; Simonsen, J.; Glasius, M.; Wåhlin, P.; Raaschou-Nielsen, O.; Loft, S. Exposure to Ultrafine Particles from Ambient Air and Oxidative Stress–Induced DNA Damage. *Environ. Health Perspect.* **2007**, *115* (8), 1177–1182.

(19) Pope, C. A.; Verrier, R. L.; Lovett, E. G.; Larson, A. C.; Raizenne, M. E.; Kanner, R. E.; Schwartz, J.; Villegas, G. M.; Gold, D. R.; Dockery, D. W. Heart Rate Variability Associated with Particulate Air Pollution. *Am. Heart J.* **1999**, *138* (5 Pt 1), 890–899.

(20) Robock, A. The Mount St. Helens Volcanic Eruption of 18 May 1980: Minimal Climatic Effect. *Science* **1981**, *212* (4501), 1383–1384.

(21) Ma, S. Production of Secondary Organic Aerosol from Multiphase Monoterpenes. In *Atmospheric Aerosols - Regional Characteristics - Chemistry and Physics*; INTECH, 2012; pp. 363–378.

(22) Surratt, J. D.; Gómez-González, Y.; Chan, A. W. H.; Vermeylen, R.; Shahgholi, M.; Kleindienst, T. E.; Edney, E. O.; Offenberg, J. H.; Lewandowski, M.; Jaoui, M.; et al. Organosulfate Formation in Biogenic Secondary Organic Aerosol. *J. Phys. Chem. A* **2008**, *112* (36), 8345–8378.

(23) de Leeuw, G.; Andreas, E. L.; Anguelova, M. D.; Fairall, C. W.; Lewis, E. R.; O'Dowd, C.; Schulz, M.; Schwartz, S. E. Production Flux of Sea Spray Aerosol. *Rev. Geophys.* **2011**, *49* (2), RG2001.

(24) Stenchikov, G. L.; Kirchner, I.; Robock, A.; Graf, H.-F.; Antuña, J. C.; Grainger, R. G.; Lambert, A.; Thomason, L. Radiative Forcing from the 1991 Mount Pinatubo Volcanic Eruption. *J. Geophys. Res.* **1998**, *103* (D12), 13837–13857.

(25) Dentener, F.; Drevet, J.; Lamarque, J. F.; Bey, I.; Eickhout, B.; Fiore, A. M.; Hauglustaine, D.; Horowitz, L. W.; Krol, M.; Kulshrestha, U. C.; et al. Nitrogen and Sulfur Deposition on Regional and Global Scales: A Multimodel Evaluation. *Glob. Biogeochem. Cycles* **2006**.

(26) Bond, T. C.; Streets, D. G. et. al. A Technology-Based Global Inventory of Black and Organic Carbon Emissions from Combustion. *J. Geophys. Res.* **2004**, *109*.

(27) Barresheim, H.; Elste, T.; Tremmel, H. G.; Allen, A. G.; Hansson, H. C.; Rosman, K.; Dal Maso, M.; Makela, J. M.; Kulmala, M.; O'Dowd, C. D. Gas-Aerosol Relationships of H_2SO_4, MSA, and OH: Observations in the Coastal Marine Boundary Layer at Mace Head, Ireland. *J. Geophys. Res.* **2002**, *107* (D19), 8100.

(28) Xing, J.; Wang, J.; Mathur, R.; Pleim, J.; Wang, S.; Hogrefe, C.; Gan, C.-M.; Wong, D. C.; Hao, J. Unexpected Benefits of Reducing Aerosol Cooling Effects. *Environ. Sci. Technol.* **2016**, *50* (14), 7527–7534.

(29) Xue, J.; Yuan, Z.; Griffith, S. M.; Yu, X.; Lau, A. K. H.; Yu, J. Z. Sulfate Formation Enhanced by a Cocktail of High NO_x, SO_2, Particulate Matter, and Droplet pH during Haze-Fog Events in Megacities in China: An Observation-Based Modeling Investigation. *Environ. Sci. Technol.* **2016**, *50* (14), 7325–7334.

(30) Lu, Z.; Streets, D. G.; Zhang, Q.; Wang, S.; Carmichael, G. R.; Cheng, Y. F.; Wei, C.; Chin, M.; Diehl, T.; Tan, Q. Sulfur Dioxide Emissions in China and Sulfur Trends in East Asia since 2000. *Atmos. Chem. Phys.* **2010**, *10* (13), 6311–6331.

(31) Wang, Y.; Zhuang, G.; Zhang, X.; Huang, K.; Xu, C.; Tang, A.; Chen, J.; An, Z. The Ion Chemistry, Seasonal Cycle, and Sources of $PM_{2.5}$ and TSP Aerosol in Shanghai. *Atmos. Environ.* **2006**, *40* (16), 2935–2952.

(32) Rumsey, I. C.; Aneja, V. P.; Lonneman, W. A. Characterizing Reduced Sulfur Compounds Emissions from a Swine Concentrated Animal Feeding Operation. *Atmos. Environ.* **2014**, *94*, 458–466.

(33) Lamb, B.; Westberg, H.; Allwine, G.; Bamesberger, L.; Guenther, A. Measurement of Biogenic Sulfur Emissions from Soils and Vegetation: Application of Dynamic Enclosure Methods with Natusch Filter and GC/FPD Analysis. *J. Atmos. Chem.* **1987**, *5* (4), 469–491.

(34) Kim, K. Y.; Ko, H. J.; Kim, H. T.; Kim, Y. S.; Roh, Y. M.; Lee, C. M.; Kim, H. S.; Kim, C. N. Sulfuric Odorous Compounds Emitted from Pig-Feeding Operations. *Atmos. Environ.* **2007**, *41* (23), 4811–4818.

(35) Kuhn, U.; Sintermann, J.; Spirig, C.; Jocher, M.; Ammann, C.; Neftel, A. Basic Biogenic Aerosol Precursors: Agricultural Source Attribution of Volatile Amines Revised. *Geophys. Res. Lett.* **2011**, *38* (16), L16811.

(36) Kinne, S.; Schulz, M.; Textor, C.; Guibert, S.; Balkanski, Y.; Bauer, S. E.; Berntsen, T.; Berglen, T. F.; Boucher, O.; Chin, M.; et al. An AeroCom Initial Assessment – Optical Properties in Aerosol Component Modules of Global Models. *Atmos. Chem. Phys.* **2006**, *6* (7), 1815–1834.

(37) Huang, X.; Zhao, Q.; He, L.; Hu, M.; Bian, Q.; Xue, L.; Zhang, Y. Identification of Secondary Organic Aerosols Based on Aerosol Mass Spectrometry. *Sci. China Chem.* **2010**, *53* (12), 2593–2599.

(38) McComiskey, A.; Feingold, G. The Scale Problem in Quantifying Aerosol Indirect Effects. *Atmos. Chem. Phys.* **2012**, *12* (2), 1031–1049.

(39) Volkamer, R.; Jimenez, J. L.; San Martini, F.; Dzepina, K.; Zhang, Q.; Salcedo, D.; Molina, L. T.; Worsnop, D. R.; Molina, M. J. Secondary Organic Aerosol Formation from Anthropogenic Air Pollution: Rapid and Higher than Expected. *Geophys. Res. Lett.* **2006**, *33* (17), L17811.

(40) Molina, M. J.; Rowland, F. S. Stratospheric Sink for Chlorofluoromethanes: Chlorine Atom-Catalysed Destruction of Ozone. *Nature* **1974**, *249* (5460), 810–812.

(41) Smith, J. N.; Barsanti, K. C.; Friedli, H. R.; Ehn, M.; Kulmala, M.; Collins, D. R.; Scheckman, J. H.; Williams, B. J.; McMurry, P. H. Observations of Aminium Salts in Atmospheric Nanoparticles and Possible Climatic Implications. *Proc. Natl. Acad. Sci. USA* **2010**, *107* (15), 6634–6639.

(42) Murphy, S. M.; Sorooshian, A.; Kroll, J. H.; Ng, N. L.; Chhabra, P.; Tong, C.; Surratt, J. D.; Knipping, E.; Flagan, R. C.; Seinfeld, J. H. Secondary Aerosol Formation from Atmospheric Reactions of Aliphatic Amines. *Atmos. Chem. Phys.* **2007**, *7* (9), 2313–2337.

(43) Sorooshian, A.; Murphy, S. M.; Hersey, S.; Gates, H.; Padro, L. T.; Nenes, A.; Brechtel, F. J.; Jonsson, H.; Flagan, R. C.; Seinfeld, J. H. Comprehensive Airborne Characterization of Aerosol from a Major Bovine Source. *Atmos. Chem. Phys.* **2008**, *8* (17), 5489–5520.

(44) Pratt, K. A.; Hatch, L. E.; Prather, K. A. Seasonal Volatility Dependence of Ambient Particle Phase Amines. *Environ. Sci. Technol.* **2009**, *43* (14), 5276–5281.

(45) Barnes, I.; Wiesen, P.; Gallus, M. Rate Coefficients for the Reactions of OH Radicals with a Series of Alkyl-Substituted Amines. *J. Phys. Chem. A* **2016**, *120* (44), 8823–8829.

(46) Schade, G. W.; Crutzen, P. J. Emission of Aliphatic Amines from Animal Husbandry and Their Reactions: Potential Source of N_2O and HCN. *J. Atmos. Chem.* **1995**, *22* (3), 319–346.

(47) Dawson, M. L.; Varner, M. E.; Perraud, V.; Ezell, M. J.; Gerber, B.; Finlayson-Pitts, B. J. Simplified Mechanism for New Particle Formation from Methanesulfonic Acid, Amines, Andwater via Experiments and Ab Initio Calculations. *Proc. Natl. Acad. Sci. USA* **2012**, *109* (46), 18719–18724.

(48) Chen, H.; Ezell, M. J.; Arquero, K. D.; Varner, M. E.; Dawson, M. L.; Gerber, R. B.; Finlayson-Pitts, B. J. New Particle Formation and Growth from Methanesulfonic Acid, Trimethylamine and Water. *Phys. Chem. Chem. Phys.* **2015**, *17*, 13699–13709.

(49) Nielsen, C. J.; D'Anna, B.; Karl, M.; Aursnes, M.; Boreave, A.; Bossi, R.; Coldevin Bunkan, A. J.; Glasius, M.; Kaldal Hansen, A. M.; Hallquist, M.; et al. *Summary Report: Photo-Oxidation of Methylamine, Dimethylamine and Trimethylamine*; Atmospheric Degradation of Amines; Summary report CLIMIT project no. 201604; NIAR, 2011.

(50) Silva, P. J.; Erupe, M. E.; Price, D.; Elias, J.; G. J. Malloy, Q.; Li, Q.; Warren, B.; Cocker, D. R. Trimethylamine as Precursor to Secondary Organic Aerosol Formation via Nitrate Radical Reaction in the Atmosphere. *Environ. Sci. Technol.* **2008**, *42* (13), 4689–4696.

(51) Chen, H.; Varner, M. E.; Gerber, R. B.; Finlayson-Pitts, B. J. Reactions of Methanesulfonic Acid with Amines and Ammonia as a Source of New Particles in Air. *J. Phys. Chem. B* **2016**, *120* (8), 1526–1536.

(52) Cocker, D. R.; Flagan, R. C.; Seinfeld, J. H. State-of-the-Art Chamber Facility for Studying Atmospheric Aerosol Chemistry. *Environ. Sci. Technol.* **2001**, *35* (12), 2594–2601.

(53) Zhang, X.; Cappa, C. D.; Jathar, S. H.; McVay, R. C.; Ensberg, J. J.; Kleeman, M. J.; Seinfeld, J. H. Influence of Vapor Wall Loss in Laboratory Chambers on Yields of Secondary Organic Aerosol. *Proc. Natl. Acad. Sci. USA* **2014**, *111* (16), 5802–5807.

(54) Grosjean, D. Wall Loss of Gaseous Pollutants in Outdoor Teflon Chambers. *Environ. Sci. Technol.* **1985**, *19* (11), 1059–1065.

(55) Kristensen, K.; Jensen, L. N.; Glasius, M.; M. Bilde. The Effect of Sub-Zero Temperature on the Formation and Composition of Secondary Organic Aerosol from Ozonolysis of Alpha-Pinene. *Environ. Sci. Process. Impacts* **2017**, *19* (10), 1220–1234.

(56) Pöschl, U.; Rudich, Y.; Ammann, M. Kinetic Model Framework for Aerosol and Cloud Surface Chemistry and Gas-Particle Interactions – Part 1: General Equations, Parameters, and Terminology. *Atmos. Chem. Phys.* **2007**, *7* (23), 5989–6023.

(57) Yin, F.; Grosjean, D.; Seinfeld, J. H. Photooxidation of Dimethyl Sulfide and Dimethyl Disulfide. I: Mechanism Development. *J. Atmos. Chem.* **1990**, *11* (4), 309–364.

(58) Wolfram Research, Inc. *Mathematica*; Wolfram Research, Inc.: Champaign, Illinois, 2017.

(59) Bunkan, A. J. C.; Hetzler, J.; Mikoviny, T.; Wisthaler, A.; Nielsen, C. J.; Olzmann, M. The Reactions of N-Methylformamide and N,N-Dimethylformamide with OH and Their Photo-Oxidation under Atmospheric Conditions: Experimental and Theoretical Studies. *Phys. Chem. Chem. Phys.* **2015**, *17* (10), 7046–7059.